This is a repository copy of *On the biaxiality of smectic C and ferroelectric liquid crystals*.

Article:

On the biaxiality of smectic C and ferroelectric liquid crystals

J.C. Jones

School of Physics and Astronomy, University of Leeds, Leeds, LS2 9JT, United Kingdom

j.c.jones@leeds.ac.uk

On the biaxiality of smectic C and ferroelectric liquid crystals

Ferroelectric liquid crystals (FLC) were a major topic for research in the 1980s and 1990s to which George Gray and his research family played a fundamental role in developing the field. The famous symbiotic relationship between the chemists at Hull University and device physicists at RSRE continued throughout this period, providing the basis for the τV_{min} mode of FLC operation. The principal of this mode relies on the dielectric biaxiality inherent to the smectic C and ferroelectric smectic C* liquid crystal phases. As with nematics before, new materials and device physics developed hand-in-hand, allowing materials to be formulated with addressing times of 12μs at voltages below 30V. After reviewing the material physics behind these devices new measurements of the biaxial refractive indices and permittivities are presented, from which the biaxial order parameter C is determined.

1.   Introduction

Having enrolled for an external Doctorate with Professor George Gray at the University of Hull at the beginning of 1986, and taking until May 1991 to submit, I am privileged to be amongst George's last Ph.D. Students. As such, I think it fitting for me to contribute to this special issue commemorating George, though of course that does not detract from the great honour of this invitation nor to that I already have from having worked with one of the greatest chemists of the twentieth century.

The story begins when I first met Peter Raynes from the *Royal Signals and Radar Establishment* (*RSRE*) in Malvern, UK in June 1985. I had done my physics undergraduate project on relating nematic order parameters to display performance, and was seeking a career in liquid crystals. Peter recommended me for interviews with Cyril Hilsum from the *Hirst Research Centre, GEC* in Wembley, and Ben Sturgeon of *BDH Chemicals* in Poole. These interviews were both testing experiences, particularly as both gentlemen were giants of their fields: Cyril was famed for initiating the UK's flat panel display research programme centred on *RSRE*, and Ben for commercialising the cyano-biphenyls that had already begun to revolutionise the world of electronic displays. I was offered, and decided to take, the position from *GEC*, working on Ferroelectric Liquid Crystals (FLC), but with a secondment to *RSRE*. This was at the beginning of the UK's *JOERS / Alvey* research project between *Thorn EMI, Standard Telecommunication Laboratories (STL), BDH, RSRE* and the Chemistry Department at Hull University, which aimed to apply FLC to highly multiplexed, high speed passively addressed liquid crystal displays [1]. *GEC* were not included in this project, but also aspired to be amongst the first companies to commercialise what seemed at the time the most exciting of new LC technologies since the invention of the Twisted Nematic LCD some twelve years earlier. Creating this secondment to *RSRE* would help ensure that GEC remained close to *RSRE* (a civil service organisation working to the benefit of the British public) and its work on ferroelectric liquid crystals. However, that relationship would be strengthened greatly by also enrolling me as the secondee for an external doctorate with George in the Department of Chemistry at Hull.

A minor problem with this arrangement was that I was a physicist. Meeting George for the first time was not like my earlier interviews. Of course, I was in awe of his achievements: I had read several of his books as an undergraduate, and was conscious of his important role in worldwide liquid crystal research. The twinkle of the eye he shared with both Cyril and Ben, but he had convivial warmth too that led us quickly to be joking about which came first "the physics or the material". After George left Hull in 1998 and John Goodby took over as my external supervisor, I would only see George each spring at the annual British Liquid Crystal Conference. However, we remained friends throughout and in

2000 he honoured me through an invitation onto the editorial board of the journal *Liquid Crystals*.

Ironically, given that I was working for *GEC*, my doctoral work led to the prove that the τV_{min} mode of FLC device operation that had been developed by the *JOERS Alvey* collaboration was caused by the dielectric biaxiality of the smectic C and ferroelectric smectic C* phases [2]. As will be described, this enabled a better understanding of those devices and the invention of improved FLC materials at Hull. After the *JOERS/Alvey* collaboration, academic research into ferroelectric liquid crystals in the UK blossomed through the support of the Smectic C Physics and Materials consortium. This was organised by the Defence Evaluation and Research Agency (DERA, as RSRE had then become) bringing together and funding students for UK Mathematicians, Physicists, Chemists to discuss problems related to FLC device engineering. The team included John Goodby (Hull Chemistry), Jones (DERA), Frank Leslie (Strathclyde Mathematics), Rob Richardson (Bristol Physical Chemistry), Roy Sambles (Exeter Physics) and Tim Sluckin (Southampton Mathematics). In the mid 1990s this work was done alongside a major project between DERA, the Sharp Corporation of Japan and Sharp Laboratories Europe. The aim was to achieve full-colour video-rate operation from a passive matrix addressed FLC operating in the τVmin mode. The work from the whole of this period will be reviewed in the present paper, followed by a more detailed investigation of the material physics behind the display mode and in particular a look at the biaxial order parameters of the smectic C and FLC phases.

Although George was no longer directly involved in the later stages of the programme, his influence was strongly felt in the consortium, which followed the cooperative relationship of liquid crystal science from synthesis to physics to theory to synthesis, the same relationship that George had so actively promoted in the decades before. Today, ferroelectric liquid crystals in displays have largely been supplanted by the widespread adoption of TFT driven nematic liquid crystals. However, biaxiality and biaxial phases remain an area of intense interest in the field of liquid crystals. The search for biaxial nematics, and the profusion of biaxial and polar smectic phases based on bent-core molecules continues to excite to this day, and excitement that I am sure would be shared by George.

2.   Ferroelectric liquid crystal device physics

2.1   Introduction

It was well understood by the members of the JOERS/Alvey consortium in the mid-1980s that introducing a new liquid crystal display technology would require a close interaction between chemists, physicists and engineers. George's group at Hull was the natural choice for synthesising new ferroelectric liquid crystals, not just because of the international reputation for excellence of the group, but also because of the long-standing ability to conduct application-driven science. Before new mixtures could be devised, methods for achieving the appropriate liquid crystal alignment, measuring the appropriate physical properties and an understanding of their relationship with device performance were required.

The basic requirements for device operation were present in the original work of Clark and Lagerwall in 1980 [3], shown schematically in figure 1. Bistability results on cooling from an aligned smectic A (S_A) phase into the chiral smectic C* (S_C*) if the sample is sufficiently thin to unwind the S_C* helical pitch. Latching between the states occurs for DC pulses of opposing polarity coupling to the ferroelectric spontaneous polarisation $\mathbf{P_s}$, with an orientation dictated by the sign of $\mathbf{P_s}$ for the material. Optical contrast is derived from crossed polarisers arranged so that the director is parallel to the polariser or analyser in the black state. The white state results if the director is switched through about 45° in the cell plane and the cell gap d is arranged to give a multiple of the half-wave condition for green light: $\Delta n.d = (m + 1/2)\lambda$. The S_C* cone angle θ_c is typically about 22.5° so that the director switches through $2\theta_c$, which is close to the optimum angle 45°. Typical materials have a birefringence $\Delta n \approx 0.13$ and the device latches between black and white states when the cell gap d $\approx 2\mu m$. The surface stabilised state, with its unwound S_C* helix, was then achieved using materials with a pitch P > 4d $\approx 8\mu m$.

Ignoring the effect of the dielectric anisotropies, the latching torque is related directly to $\mathbf{P_s} \times \mathbf{E}$, giving an approximate response time of:

$$\tau = \frac{\gamma_1 \sin^{-1}\theta_C}{|\boldsymbol{P_s}|E} \qquad\qquad (1)$$

Typical values for FLC materials are rotational viscosity $\gamma_1 \approx 0.25$ Pa.s and $\boldsymbol{P_S} = 50$ nCcm^{-2}, giving a predicted response time between states of 15µs for a |10V| signal. This response time is very fast for a liquid crystal display, being thousands of times faster than a typical nematic device. This feature helped drive the worldwide interest in FLC displays throughout the 80s and 90s. However, it is important to note that the speed useful not only for displays, but for spatial light modulators used in telecommunications, and optical shutters used for camera viewfinders and projection displays.

The other property of the Clark and Lagerwall arrangement that is useful for displays is bistability. With the device of figure 1, the bistability is dictated by the surfaces. As throughout the bulk, the surface director is constrained to lie on the S_C* cone of possible orientations: it cannot simultaneously lie at the preferred pre-tilt and azimuthal direction. Given the out-of-plane or zenithal anchoring energy W_θ is typically an order of magnitude greater than the in-pane azimuthal anchoring W_β, then the director profile from one surface to the next is uniform director, lying in the plane of the cell and at azimuthal angles $+\theta_c$ and $-\theta_c$ to the direction of the layer normal. The energy barrier between the two states is related to W_θ / W_β. There is no energy barrier if $W_\theta = W_\beta$ and the device becomes mono-stable and exhibits so-called "V-shaped switching" [4].
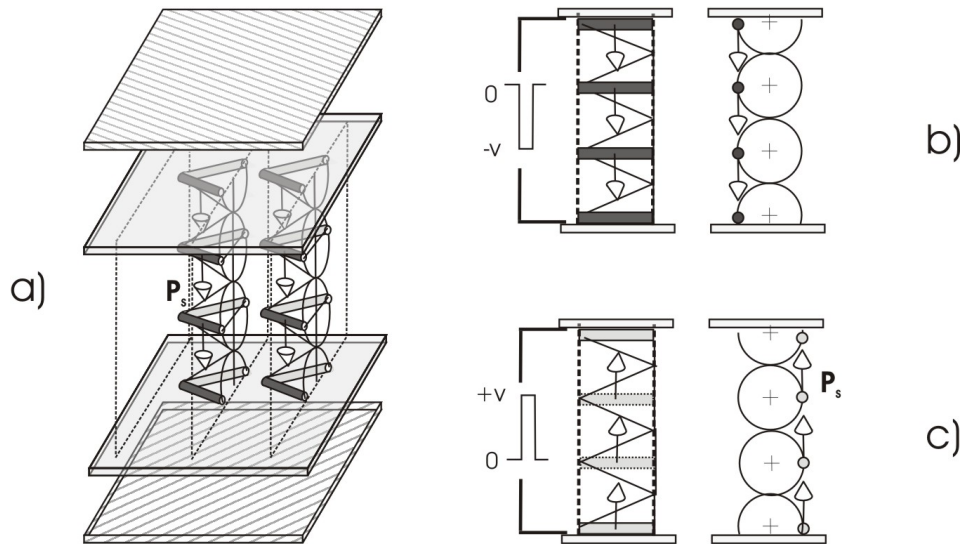
Figure 1   ***a) Surface stabilised Ferroelectric liquid crystal in the "Bookshelf" geometry. Orientation of the director after the application of b) a positive pulse of sufficient impulse and c), a negative pulse.***

2.2   *Alignment*

The devices constructed in reference [3] were fabricated by shearing the upper and lower surfaces to ensure that the smectic layers were uniform, and normal to the substrates and the shear direction. Such a method is not suited to large-scale manufacture, where the desired alignment is obtained through appropriate surface alignment treatments. Standard rubbed polymer alignment is used, with the alignment directions oriented parallel on the two substrates. However, cells made with such an arrangement clearly deviated from the arrangement of figure 1, as indicated by the photo-micrographs of a 3μm spaced racemic sample of the commercial ferroelectric liquid crystal SCE8 [5] shown in figure 2. Although the sample exhibits two domains as expected for the bookshelf structure of figure 1, the extinction of white light when viewed between crossed polarisers is poor, even coloured, with a transmission minimum occurring at an angle less than half the expected value of θ_c. Moreover, devices usually show sharp zigzag defects, which are not influenced by ferroelectric

switching of the domains. The colouration either side of the defects differs somewhat, even for orientations where the layers are oriented parallel to one of the polarisers so that the two domains are indistinguishable, figure 2b.

Understanding this behaviour requires consideration of the smectic layer structure first, and then the director profile of the sample. Figure 3a shows a schematic of the smectic layers in a parallel-aligned sample with a surface pre-tilt θ_s of a few degrees. Even with a substantial director pre-tilt causing splay/bend in the aligned nematic phase, the divergence of the bend elastic constant K_{33} as the sample cools towards the smectic phase leads to a uniform layer structure. If the pre-tilt on the opposing surfaces is the same, then the S_A layers are formed with the layer normal in the plane of the cell and parallel to the rubbing direction *r*, as shown in figure 3a. As the sample is cooled further into the S_C* phase, the layers tilt in opposite directions in the upper and lower halves of the display, forming a symmetric chevron layer structure [6]. X-ray studies, figure 3b, show that the layer tilt ($\pm\delta$) is uniform throughout the bulk of the device, meeting in a sharp cusp at the central plane. For cells with a finite pre-tilt, there are two orientations of chevron layer structure termed C1 and C2 [7] shown in figures 2 and 3. The C1 state is the first to form on cooling from the S_A and the layer normal tilts in the same direction as the surface pre-tilt. Further cooling often causes the C2 chevron state to form, mediated by the zigzag defects. Although still a symmetric kink the layers of the C2 state tilt in the opposite direction to the preferred surface orientation of the director. Poorly aligned samples, such as those shown in figure 2, have areas of C1, areas of C2 and zigzag defects. Ensuring uniform defect-free alignment, either C1 or C2 depending on the approach chosen, is essential for display applications and for accurate measurement of the material properties. This is done by choosing the alignment surfaces, in particular the correct surface pre-tilt θ_S, zenithal anchoring W_θ and azimuthal W_β, anchoring energies [8].
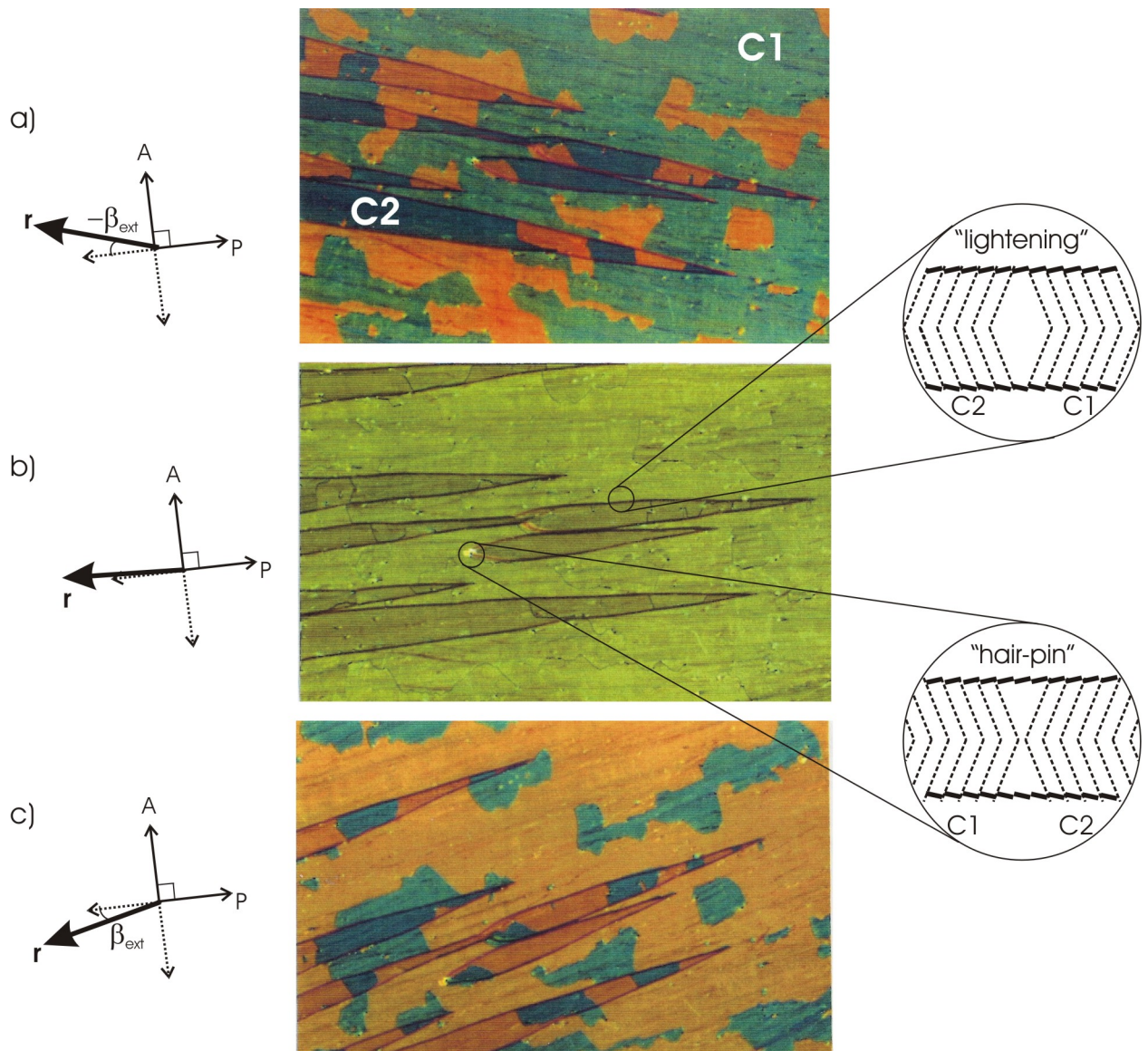
*Figure 2. Texture of a Smectic C sample (racemic SCE8) in a parallel-aligned cell with a pretilt of 2°. Zigzag defects dividing areas of C1 and C2 chevron layer alignment. A relatively thick ($\Delta n.d \approx 500nm$) sample is viewed between crossed polariser **P** and analyser **A** with the orientations a) **P** at white light extinction angle $\boldsymbol{\beta}_{ext} \approx +15°$ to the rubbing direction r, b) **P** and r parallel; and, c) **P** at $\boldsymbol{\beta}_{ext} \approx -15°$ to r.*
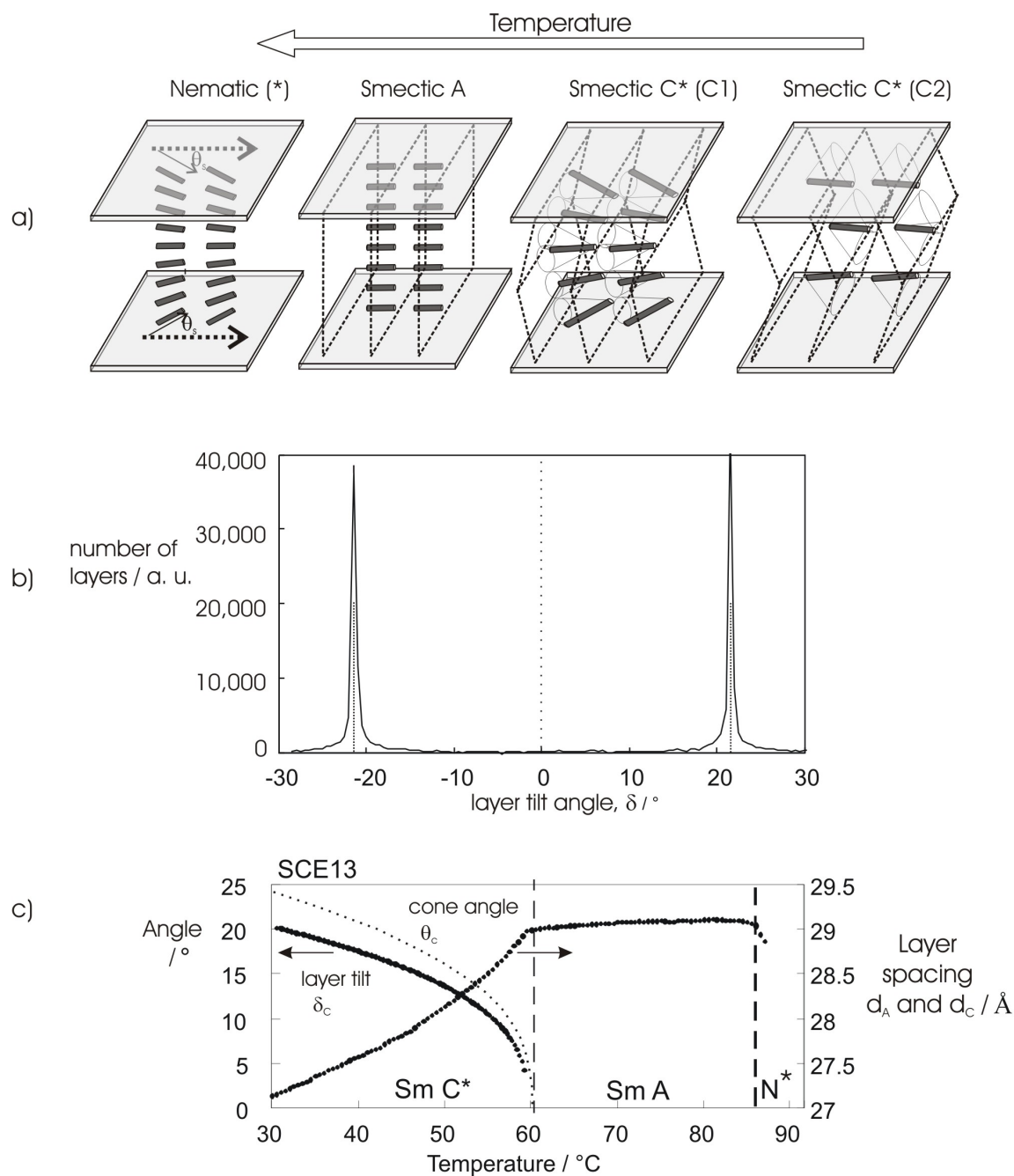
Figure 3. Formation of "chevron" layer structures on cooling a parallel-aligned planar homogenous sample through the nematic-Smectic A to Smectic C* sequence. a) Formation of C1 and C2 layer tilt; b) Smectic layer distribution at 30°C for the commercial FLC mixture SCE13 determined by X-ray diffraction; c) Temperature dependence of the layer spacing, layer tilt and optical cone angle.

The S_A to S_C^* phase transition is second order, and properties such as the S_C or S_C^* (denoted as $S_C(*)$ and used wherever the chirality of the phase is not relevant). cone angle θ_C have a critical temperature dependence approximated by the first term of the Landau-de Gennes expansion:

$$\theta_C = \theta_C \left(1 - \frac{T}{T_C}\right)^{\nu_o} \qquad , \qquad (2)$$

where T_C is the S_A to $S_C(*)$ transition temperature. The S_C layer spacing will also have a similar temperature dependence, as shown in figure 3c. At some temperature in the S_A phase, the periodicity of the layers intersecting with the surface is d_A. Rather than create new layers as the sample cools, the layers tilt instead with a $S_C(*)$ layer tilt δ_C related to the change in layer spacing as given by:

$$\theta_C = \pm \cos^{-1}\left(\frac{d_C(T)}{d_A}\right) = \delta_C\left(1 - \frac{T}{T_C}\right)^{\nu_L} \qquad , \qquad (3)$$

where d_A and $d_C(T)$ are the layer periodicities for the S_A and $S_C(*)$ phases, respectively. Figure 3c shows the temperature dependence of the layer spacing and resultant tilt angle d_C for the commercial FLC mixture SCE13 [5,9], together with the S_C cone angle θ_C. The best fits for this mixture give $\theta_0 = (52 \pm 2)°$; $\nu_O = 0.33 \pm 0.02$; $\delta_0 = (47 \pm 2)°$; $\nu_L = 0.35 \pm 0.02$. The mixture SCE8 has also been characterised [10], and the best fits found to be $\theta_0 = (47 \pm 2)°$; $\nu_O = 0.31 \pm 0.02$; $\delta_0 = (37 \pm 2)°$; $\nu_L = 0.26 \pm 0.02$, with $T_C = (60.0 \pm 0.2)°C$. For these and many other mixtures studied, δ_C/θ_C is constant and independent of temperature within experimental error, typically in the range $0.85 \leq \delta_C/\theta_C \leq 0.90$.

For surfaces without pre-tilt, $\theta_S \approx 0°$, both signs of layer tilt, C1 and C2, are favoured equally and the device will be covered with zigzags. High pre-tilt surfaces give C1 arrangement, whereas samples with intermediate pre-tilts initially cool C1 and then form the C2 state as the sample cools. These processes are readily understood by

considering the surface energy of the director, which is constrained to lie on a tilted cone. The in-plane β and out-of-plane θ components of the $S_C(*)$ **n** director are given by simple trigonometry[11]:
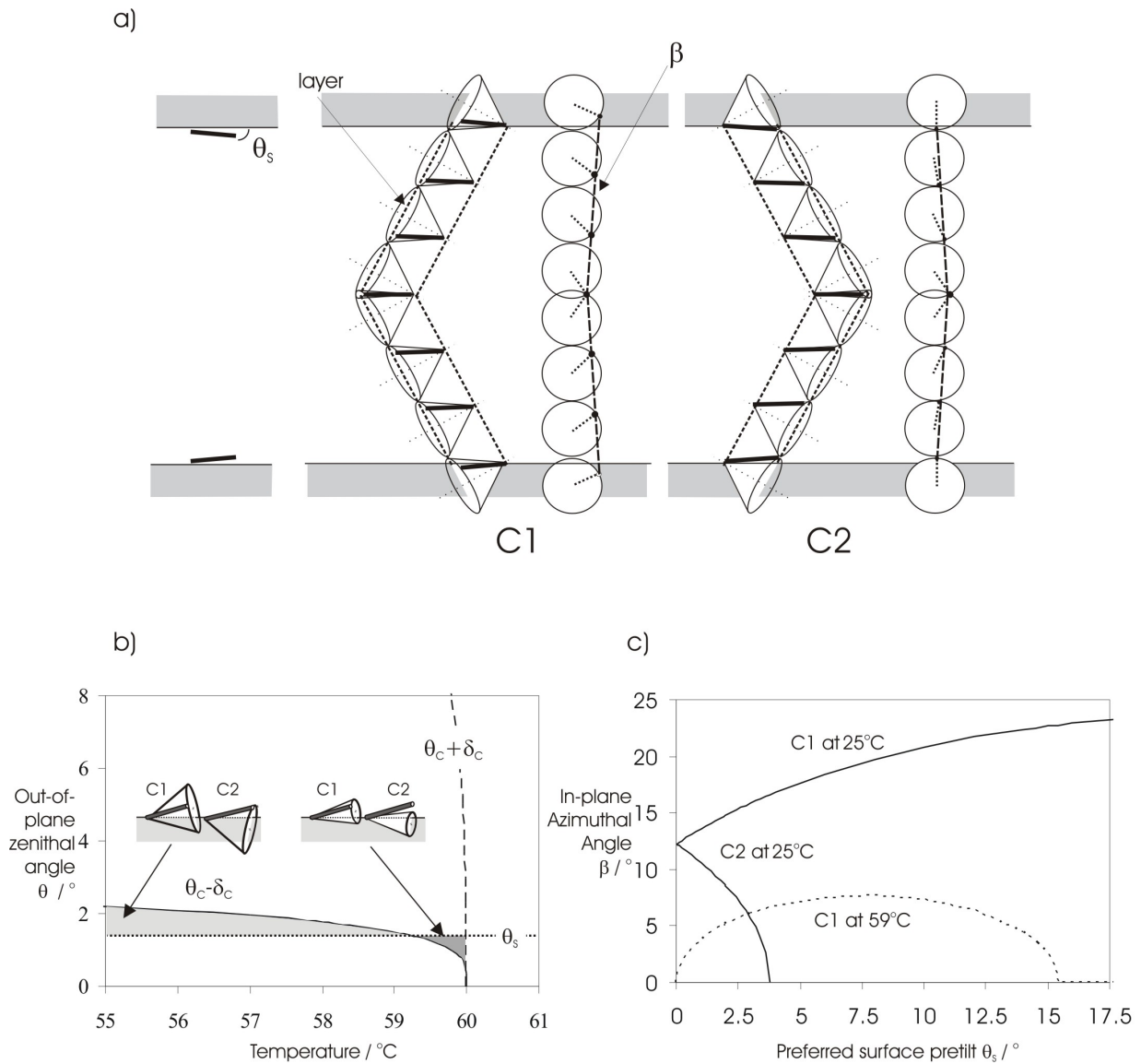
$$\beta = \tan^{-1}\left(\frac{\cos\phi_C \sin\theta_C}{\sin\phi_C \sin\delta_C \sin\theta_C + \cos\delta_C \cos\theta_C}\right) \quad , \quad (4)$$

$$\theta = \sin^{-1}\left(\sin\phi_C \cos\delta_C \sin\theta_C - \sin\delta_C \cos\theta_C\right) \quad . \quad (5)$$

The surface free energy is related to the anchoring energies and pre-tilt through:

$$G_S = W_\theta \sin^2(\theta - \theta_S) + W_\beta \sin^2\beta \quad . \quad (6)$$

If the zenithal surface anchoring is far stronger than the azimuthal, $W_\theta \gg W_\beta$, the director at the surfaces will lie at the pre-tilt θ_S. Equation (5) has solutions for pre-tilts $0 \le \theta_S \le (\theta_C + \delta_C)$ with the C1 chevron, and $0 \le \theta_S \le (\theta_C - \delta_C)$ with C2. Because the cone and layer angles follow the critical temperature dependences of equations (2) and (3), both θ_C and δ_C are small immediately below T_C and lower than the typical pre-tilt. The C2 state cannot form because $(\theta_C - \delta_C)$ is much lower than θ_S, which is closer to $(\theta_C + \delta_C)$, so that the C1 state is strongly favoured. It is the second order nature of the smectic A to smectic C* phase transition that dictates that the C1 state always forms first on cooling a sample with a finite surface pre-tilt. As $\theta_C - \delta_C$ increases with further cooling, the C2 state becomes possible at a temperature close to that where the condition $\theta_C - \delta_C = \theta_S$, figure 4. The layer transition from C1 to C2 is driven by the effect of the finite azimuthal anchoring energy, W_β. Except where $\theta_S = \theta_C \pm \delta_C$, the director has an out-of-plane azimuthal angle β dictated by equation (4), assuming soft-mode changes of θ_C are energetically more costly than deviations from the surface energies. Figure 4c shows the out-of-plane azimuth angle plotted for SCE8 at $T_C - T =$

Figure 4. The relationship between surface pre-tilt and smectic C (*) layer orientation. a) Schematic of the director profiles for parallel-aligned surfaces with pretilt θ_S in the C1 and C2 chevron arrangements; of surface pretilt on the layer and director profiles; b) Temperature dependence of the zenithal angle limits for SCE8. Also shown are schematics for the C1 and C2 surface orientation at temperatures close to T_C and well below; c) The azimuthal angle for SCE8 in the C1 and C2 states for T = 59°C (T_C-T=1°C) and 25°C (T_C-T=35°C). Note, there is no solution for the C2 close to the phase transition.

1°C and T_C-T = 35°C for various out-of-plane tilts θ. In the C1 state, the azimuthal angle, and hence the energetic cost related to W_β, increases as the cone angle and layer tilt angle increase on cooling. At the temperature where θ_C-δ_C = θ_S, the C2 state has the lower surface energy, since the surface director lies at the pre-tilt with β = 0°. If the azimuthal anchoring W_β is high, the energy advantage of the C2 is sufficiently great to cause the first-order layer reorientation from C1 to C2. In summary, formation of a uniform C1 state, requires low W_β and $\theta_S \gg \theta_C$-δ_C (typically $\theta_S \geq 12°$) whereas uniform C2 occurs when W_β is large and $\theta_S \approx \theta_C$-$\delta_C$, typically $2° \leq \theta_S \leq 6°$.

Despite the sharp discontinuity of the smectic layers and given $\delta_C \leq \theta_C$, the **n** director remains continuous across the chevron interface provided it is oriented at either of the two orientations where θ_m is maintained for both top and bottom layers (or the single orientation for the special case where $\delta_C = \theta_C$). This is best visualised as two over-lapping cones as shown in figure 5 where the face of the cones represent the layer planes and the **n**-director is confined to lie on the plane that bisects upper and lower cones. The orientation of a unit vector describing the projection of **n** into the layer plane (termed the c-director) is described by the orientation angle ϕ_i [12]:

$$\sin\phi_i = \pm\frac{\tan\delta_C}{\tan\theta_C}$$
, (7)
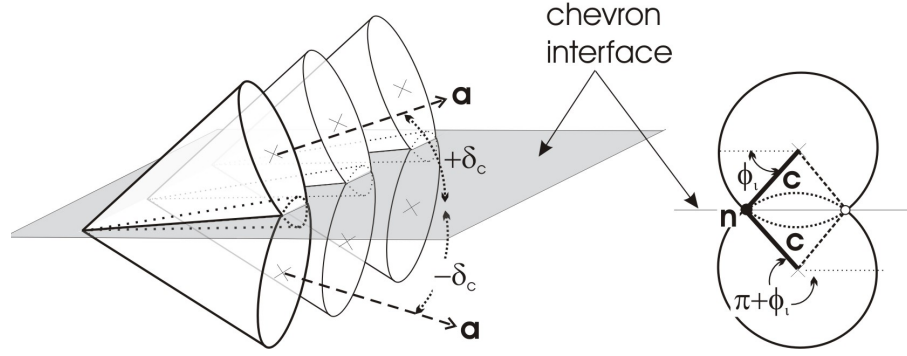
***Figure 5). The chevron interface sheet defect for smectic C and smectic C* and definition of the c-director.***

at the chevron interface and the director has a component in the plane of the chevron interface β_i given by:

$$\cos\beta_i = \pm\frac{\cos\theta_C}{\cos\delta_C}$$.   (8)

The chevron interface is the root of the $S_C(*)$ device bistability: the activation energy between the bistable states is associated with local deformation of the layers at the chevron interface as the **c**-director swaps from one orientation to the other. Application of the DC field coupling to $\mathbf{P_S}$ reorients the director towards $\phi=0$ or π, and the in-plane azimuthal angle for the **n** measured from the rubbing direction β_0 is:

$$\beta_0 = \pm\tan^{-1}\left(\frac{\tan\theta_C}{\cos\delta_C}\right)$$,   (9)

which is typically a few degrees greater than the cone angle, as shown in figure 6. Where δ_C is close to θ_C then β_i is far lower than the cone angle θ_C, typically being approximately $\beta_i \approx 0.5\theta_C$. Temporarily ignoring the effect of the surfaces, the director
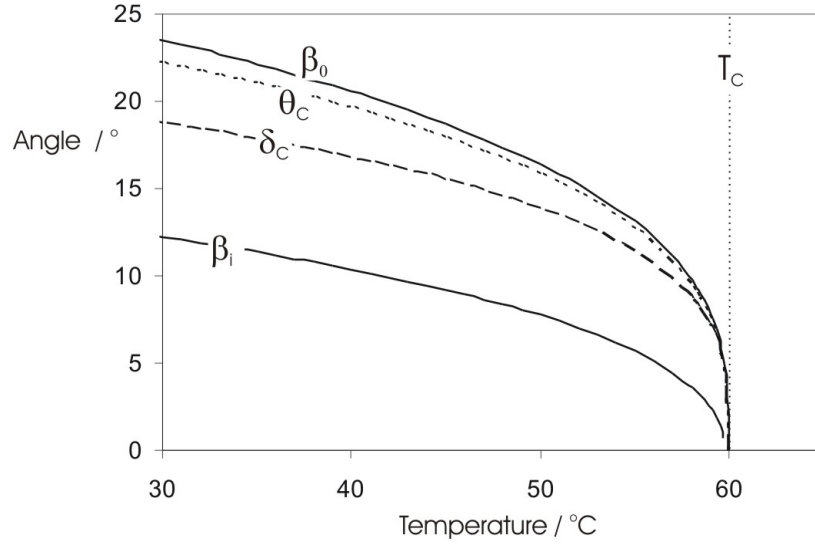
Figure 6. Temperature dependence of the SCE8 layer tilt δ_C, cone angle θ_C, azimuthal angle at the chevron interface β_i and azimuthal angle β_0 for the fully switched director oriented at the side of the cone $\phi_C = 0, \pi$.

of the bistable FLC quiescent states would be uniformly at $\pm\beta_i$. Setting crossed polarisers to give one domain black, then the director of the opposite domain is oriented at $2\beta_i \approx 22.5°$ and not the optimum 45° required for maximum transmittance. That is, the white light transmittance is reduced significantly, to approximately 50% of that required for attractive device operation.

In practice, the director at the surface will lie at some orientation upon the cone that minimises the surface and elastic deformation energies. The director profile from the surface to the chevron interface is found by solving the free energy across the cell. S_C and S_C* phase elasticity is far more complicated than that of the usual nematic phase, [13 - 15] particularly if the smectic layer compressibility is also considered [16]. Considering the case of incompressible layers alone, there are nine elastic coefficients, and the elastic free energy G_K is [15]:

16

$$G_k = \frac{1}{2} \int_V \begin{bmatrix} A_{21}(\nabla.a.)^2 + B_1(a.\nabla \times c.)^2 + B_2(\nabla.c)^2 + B_3(c.\nabla \times c)^2 \\ +(2A_{11} + A_{12} + A_{21} + B_3)(b.\nabla \times c)^2 - (2A_{11} + 2A_{21} + B_3)(\nabla.a)(b.\nabla \times c) \\ -B_{13}(a.\nabla \times c)(c.\nabla \times c) \\ +2(C_1 + C_2 - B_{13})(\nabla.c)(b.\nabla \times c.) - 2C_2(\nabla.a)(\nabla.c) \end{bmatrix} dV \quad (10)$$

where $\mathbf{b} = \mathbf{a} \times \mathbf{c}$, is the unit vector parallel to the C_2 symmetry axis, and A_{ii}, B_i and C_i are the elastic constants. Sketches for the deformations corresponding to the elastic constants B_1, B_2, B_3, A_{12} and A_{21} are shown in figure 7. For simplicity, the layer tilt
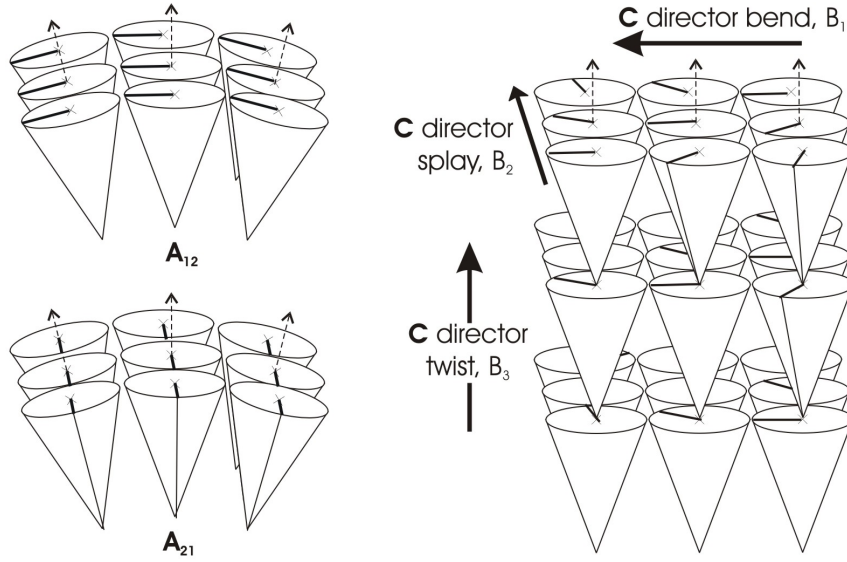
Figure 7.   Examples of smectic elasticity and sheet defects: a) Splay deformation in the S_A phase; b) S_C c-director elastic constants relating to the orientation of c with respect to layer divergence A_{12} and A_{21}, and bend, splay and twist of the c-director B_{11}, B_{22}, and B_{33}.

and cone angles are assumed uniform and invariant within the sample. Treating the chevron interface as an infinitely bound surface (so that the director elastic terms across the interface are ignored), and the director profile as uniform in the cell plans (*xy*) and described solely by the orientation angle ϕ_C changing in the *z*-direction which is normal to the cell plane, then equation (10) has solutions [10]:

$$[(B_1\sin^2\phi_C + B_2\cos^2\phi_C)\cos^2\delta_C + B_3\sin^2\delta_C - B_{13}\sin\phi\sin2\delta_C]\frac{\partial^2\phi_C}{\partial z^2} =$$

$$\frac{1}{2}\left[(B_1 - B_2)\sin2\phi_C\cos^2\delta_C - B_{13}\cos\phi_C\sin2\delta_C\right]\left(\frac{\partial\phi_C}{\partial z}\right)^2 \qquad (11)$$

Assuming that the material is elastically isotropic, $B=B_1=B_2=B_3$ and $B_{13} = 0$, then equation (11) simplifies further to:

$$B\frac{\partial^2\phi_C}{\partial z^2} = 0 \qquad\qquad , \qquad (12)$$

for which the trivial solution is:

$$\phi_C(z) = \phi_S + \frac{d}{2}\left(\phi_i - \phi_S\right) \qquad\qquad . \qquad (13)$$

This profile corresponds to the director varying linearly from the surface value of ϕ_S to the chevron interface ϕ_S, given by equation (7). The chevron interface lies in the central plane of the cell and the two surfaces are equivalent, so the profile has mirror symmetry and forms a triangular director profile (TDP) [17]. Typically, $\delta_C \approx \theta_C$, and so the in-plane component of the director β_C follows the triangular profile from β_S to β_i and back to β_S, where the azimuthal angle at the chevron interface β_i is given by equation (8). Modelling verifies [10] that the deviation from a TDP is insignificant, even for large elastic anisotropies.

The symmetric structure of the TDP leads to the imperfect white light extinction of a smectic C or FLC sample viewed between crossed polarisers, such as that evident in the photomicrographs of figure 2. This is because the extinction angle β_{ext} is wavelength λ dependent and given by [17]:

$$\tan 2(\beta_{ext} - \beta_S) = \frac{\tan\left[(\beta_i - \beta_s)\sqrt{1 + \frac{1}{4}\alpha^2}\right]}{\sqrt{1 + \frac{1}{4}\alpha^2}} \quad , \qquad (14)$$

where α ($=\pi\Delta nd/\phi\lambda$), the director twist is given by $\phi = \beta_i - \beta_S$, and the effect of the small out of plane tilt θ is ignored. At long wavelengths or low cell gaps equation (14) predicts that the extinction angle tends towards:

$$\beta_{ext} \to \frac{(\beta_i + \beta_s)}{2} \qquad . \qquad (15)$$

It also predicts that the extinction angle tends towards ± 45° for cell gaps close to the full wave plate condition ($\Delta n.d = \lambda$) at which point domains either side of the layer normal are optically equivalent. Figure 8a shows the theoretical wavelength dependence of the extinction angle for a sample with $\Delta n.d \approx 530$nm, a condition similar to that of the sample used for the photo-micrographs of figure 2. One sign of domain appears blue where the sample is oriented at the yellow extinction angle. At that orientation, the opposite domain transmits the yellow wavelengths, but extinguishes blue because of the inversion of extinction angle seen below the full wave point. Of course, the cell gap for a display will be chosen close to the half wave plate condition. For such thinner cells, the extinction angle has a weaker wavelength dependence, as predicted by equation (14) and shown in figure 8b. At the half-wave-plate condition, extinction of one domain will be black, and the other white, with an intensity I given by:
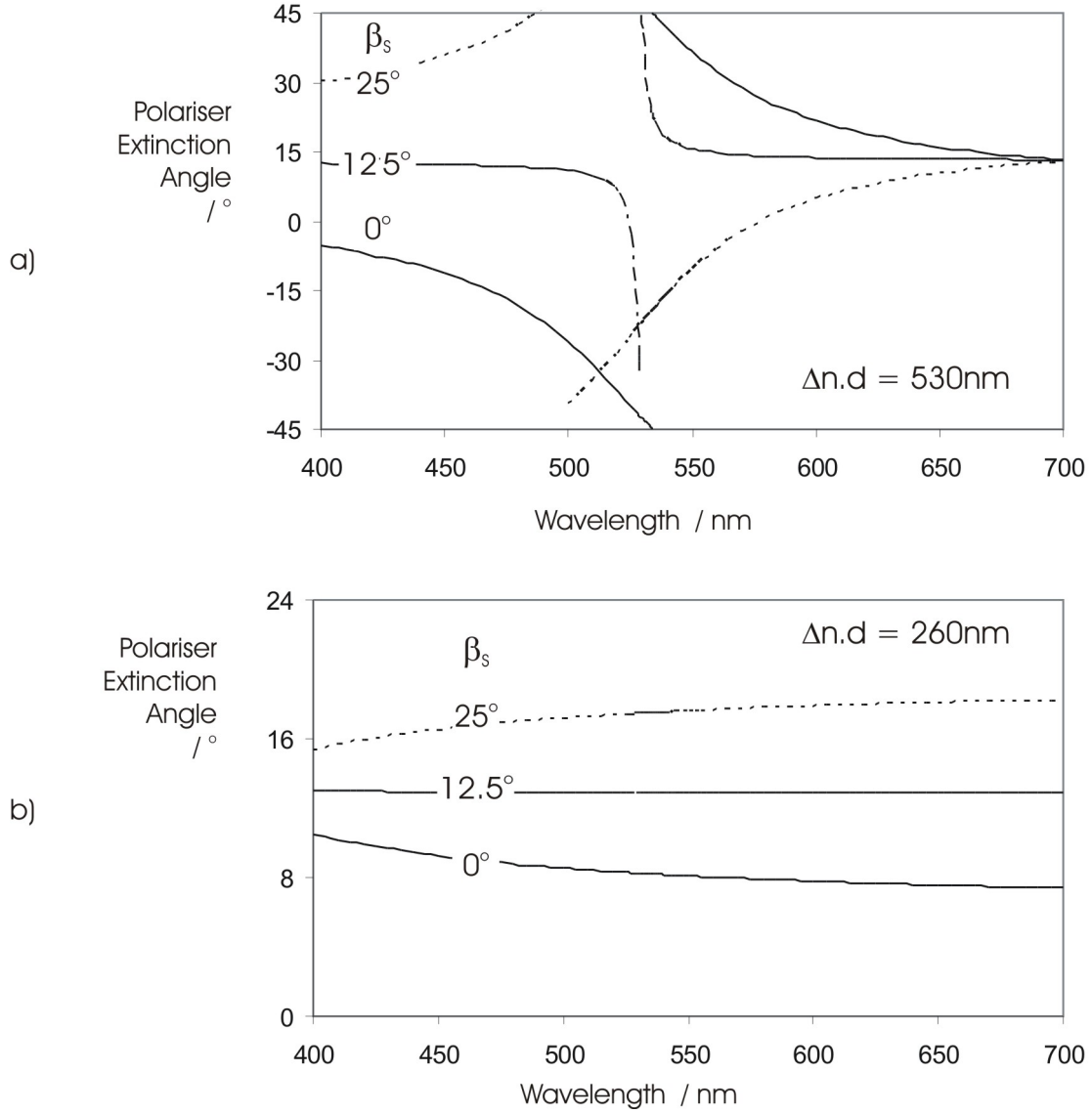
Figure 8. The optical extinction angle $\boldsymbol{\beta}_{ext}$ for chevron quiescent state with the TDP for samples with surface azimuthal angle $\boldsymbol{\beta}_S = 0°$, 12.5° and 25°.   a) Wavelength dependent extinction angle for a thick sample with $\boldsymbol{\Delta}n.d = 530nm$; b) Wavelength dependent extinction angle for a thin sample with $\boldsymbol{\Delta}n.d = 290nm$.

$$\frac{I}{I_0} = \sin^2(4\beta_{ext})\sin^2\left(\frac{\pi\Delta n_{eff}.d}{\lambda}\right) \qquad , \qquad (16)$$

where the illuminating intensity I_0 is taken after the input polariser. The extinction at $2\beta_{ext}$ from equation (15) is typically lower than the ideal of $\beta_{ext} = 22.5°$. Figure 8 also shows that the extinction angle of the two domains is strongly dependent on the surface orientation β_s, which in turn is related to the pre-tilt and sign of layer tilt (C1 or C2). Obtaining β_{ext} close to the optimum $22.5°$ requires the pre-tilt to be close to the C1 layer tilt angle, typically $\theta_s \approx 18°$. For low pre-tilts where both C1 and C2 states occur in the same sample, such as that shown in figure 2, the optical difference either side of the of the zigzag defect is solely due to the differences in surface orientation. The director will be much closer to the rubbing direction for the C2 chevron than for the C1, and hence its extinction angle is lower. Also, when oriented with polarisers parallel and crossed to the rubbing direction, less light is transmitted for the C2 TDP (because β_{ext} is lower) as is clear from the microscopic texture figure 2b.

2.3   Electro-optic behaviour

The phase biaxiality of the S_C and S_C* phases is immediately apparent when considering their structures: the tilt of the **n** director from the layer normal **a** clearly defines a plane with a C_2 symmetry axis (**a** × **n**) perpendicular to it. The symmetry of the phase is mono-clinic and the C_2 axis is the only well defined principal axis for the system, and corresponds to $\widehat{n_2}$ in figure 9. Two obvious choices for the remaining axes use either the layer normal **a** or director **n**. The latter is chosen to give continuity of the anisotropic properties when cooling into the S_C(*) phase from higher temperature uniaxial phases. Given that the optical biaxiality is negligible [18, 19] and the materials may be considered optically uniaxial with the optic axis parallel to the director, then this choice seems sensible. Hence, we choose three principal axes ($\widehat{n_1}$, $\widehat{n_2}$,$\widehat{n_3}$) with $\widehat{n_3}$ parallel to **n** as in figure 9. However, the arbitrary nature of this choice for the three principal axes should not be forgotten, and will be discussed later in the paper. Although, almost optically uniaxial, the biaxiality of other properties is not necessarily negligible and it was this realisation that helped steer the work described here.

Introducing the biaxial dielectric and ferroelectric terms for the electro-static free energy whilst ignoring terms for inertia and viscous flow and considering only changes of the **c** director orientation ϕ_C that are induced in the direction parallel to the cell normal (z) when subject to an applied field E_z in that direction, the torque equation is [10]:

a)   b)
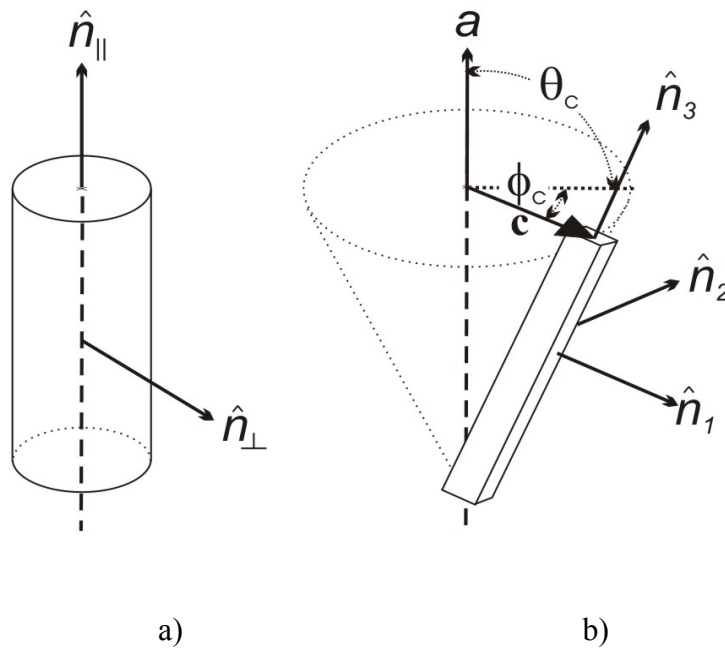
Figure 9.   ***Schematic representation of the principal axes for a) the cylindrical nematic and S_A phases and b) the monoclinic S_C. Locally, the S_C* has the same monoclinic symmetry as the achiral S_C, but becomes uniaxial about the helical precession over length scales much greater than the helical pitch.***

$$\gamma_1 \sin^2 \theta_C \frac{\partial \phi}{\partial t} = \left[\left(B_1 \sin^2 \phi_C + B_2 \cos^2 \phi_C\right)\cos^2 \delta_C + B_3 \sin^2 \delta_C - B_{13}\sin 2\delta_C \sin \phi_C\right]\frac{\partial^2 \phi_C}{\partial z^2}$$

$$+ \frac{1}{2}\left[\left(B_1 - B_2\right)\cos^2 \delta_C \sin 2\phi_C - B_{13}\sin 2\delta_C \cos \phi_C\right]\left(\frac{\partial \phi_C}{\partial z}\right)^2$$

$$+ P_S E_z \cos \delta_C \sin \phi_C - \varepsilon_o E_z^2 \partial\varepsilon \sin \phi_C \cos \phi_C \cos^2 \delta_C$$

$$- \varepsilon_o E_z^2 \Delta\varepsilon \cos \phi_C \left[\frac{1}{4}\sin 2\theta_C \sin 2\delta_C - \sin \phi_C \cos^2 \delta_C \sin^2 \theta_C\right]$$

(17)

where $\Delta\varepsilon$ is the uniaxial dielectric anisotropy (= ε_3 - ε_1) and $\partial\varepsilon$ is the dielectric biaxiality (= ε_2 - ε_1). An applied DC electric field E_z couples to $\mathbf{P_S}$ and tends to switch the device towards either $\phi_C = 0$ or $\phi_C = \pi$, depending on the relative signs of E_z and $\mathbf{Ps}$. The effect of the dielectric terms in $E_z^2\Delta\varepsilon$ and $E_z^2\partial\varepsilon$ become dominant at high field strengths; at frequencies too high to cause the ferroelectric switching response; or for achiral smectic C systems, where $\mathbf{P_S} = 0$.

Consider first the effect of the dielectric terms alone (i.e. S_C or high frequency S_C*). The AC stabilising effect of the dielectric anisotropies is similar to the switching effect in uniaxial nematic liquid crystals, but it is the effect of the dielectric biaxiality that dominates in the smectic C and FLC phases. With a negative uniaxial anisotropy, the applied field tends to reduce any out-of-plane tilt in the cell and stabilise the low memory angle state $\beta_{ext} = \beta_i$, given by equation (8). However, this is not what is found experimentally, where an applied AC field tends to increase the extinction angle towards the fully switched condition given by equation (9) and remove colouration of the domains. This is because of the effect of the positive dielectric biaxiality $\partial\varepsilon$ [20, 21], which is stronger than the negative uniaxial anisotropy $\Delta\varepsilon$. The electro-static energy is minimum at the orientation [21]:

$$\sin \phi_C = \pm\frac{\Delta\varepsilon \sin \theta_C \cos \theta_C \tan \delta_C}{\Delta\varepsilon \sin^2 \theta_C - \partial\varepsilon} \qquad\qquad , \qquad\qquad (18)$$

where the electro-static energy is reduced as the **c**-director reorients to ensure the largest permittivity e_2 has the highest component in the direction of the field. This occurs close to either condition $\phi_C = 0$ or $\phi_C = \pi$ if $\partial\varepsilon \gg |\Delta\varepsilon| \sin^2\theta_C$. This increase of extinction angle towards the fully switched condition is termed AC stabilisation [22]. Typical results for the commercial liquid crystal mixture SCE8(R) are shown in figure 10a.

Of course, the director profile will only approach the fully AC stabilised condition of equation (18) if the field is very high. At intermediate fields the director will remain pinned at the chevron-interface in the device centre, and at a surface orientation related to the anchoring energies, figure 10b. The applied AC field couples to the permittivities and distorts the director profile in the bulk of the sample away from surfaces and chevron interface. In chevron geometries the elastic restoring torque is dominated by **c**-director bend and splay, B_1 and B_2, respectively. For the C1 geometry with a high surface pre-tilt, the director profile is already close to $\phi_C = 0,\pi$ throughout much of the device, and the effect of the AC waveform is small. However, for the C2 geometry, the initial TDP structure is deformed considerably in the bulk of the cell. Indeed, ensuring that the AC stabilising effect is maximised for devices operating in the C2 geometry became a most important part of the Hull Chemistry Department FLC programme.

The effect of ferroelectricity is now considered in detail. The orientation of the spontaneous polarisation for the tilted layer geometries in the quiescent TDP state has a large component parallel to the plane of the cell, but still has domains with components either "up" or "down" with respect to the layer normal. The response to an applied DC electric field described by equation (17) is to induce reorientation of the director about the cone to maximise the component of the spontaneous polarisation parallel to the applied field. As for the case of AC stabilisation, this reorientation is constrained at the chevron interface and aligning surfaces. A DC field with the same polarity as $\mathbf{P_S}$ will cause reorientation of the director around the same side of the cone in a similar fashion to the effect of the AC stabilising field coupling to the dielectric biaxiality shown in figure 11. The director reorients to $\phi_C = 0$ or π, depending on the sign of the field and
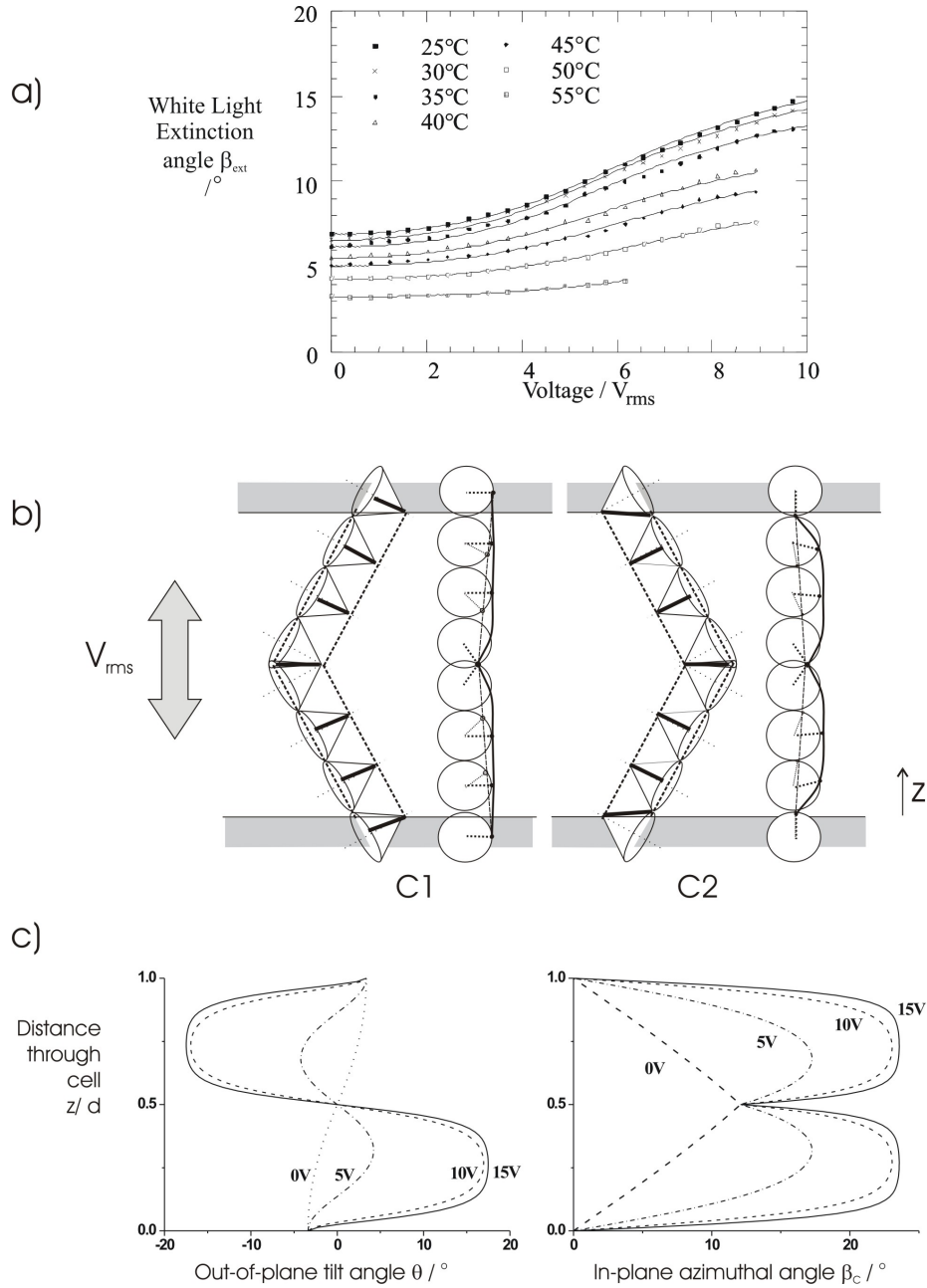
Figure 10. AC field stabilisation. a) The white light extinction angle versus applied Vrms for a 1.5μm sample of SCE8(R) in the C2 geometry at several temperatures across the smectic C range; The lines represent theoretical fits calculated using θ_C = 55.3°(1-T/T_C)^{0.32}, δ_C = 46.2°(1-T/T_C)^{0.31}, $\partial\varepsilon$ = 10.8(1-T/T_C)^{0.63}, B_1 = B_2 = 69.8pN(1-T/T_C) and T_C = 61.8°C. b) The effect of an applied AC field in high surface pre-tilt C1 and low surface pre-tilt C2 geometries; c) Theoretical predictions for the tilt and azimuthal angles for the C2 geometry with applied AC field coupling to the dielectric biaxiality

polarisation, where it remains tilted at δ_C to the applied field E_z. If very high fields are applied, the resultant torque from this tilt eventually leads to disruption of the layers and a reduction of the layer tilt angle δ_C. If this is done with a low frequency AC field, then the resulting "quasi-bookshelf" structure can be uniform [23].
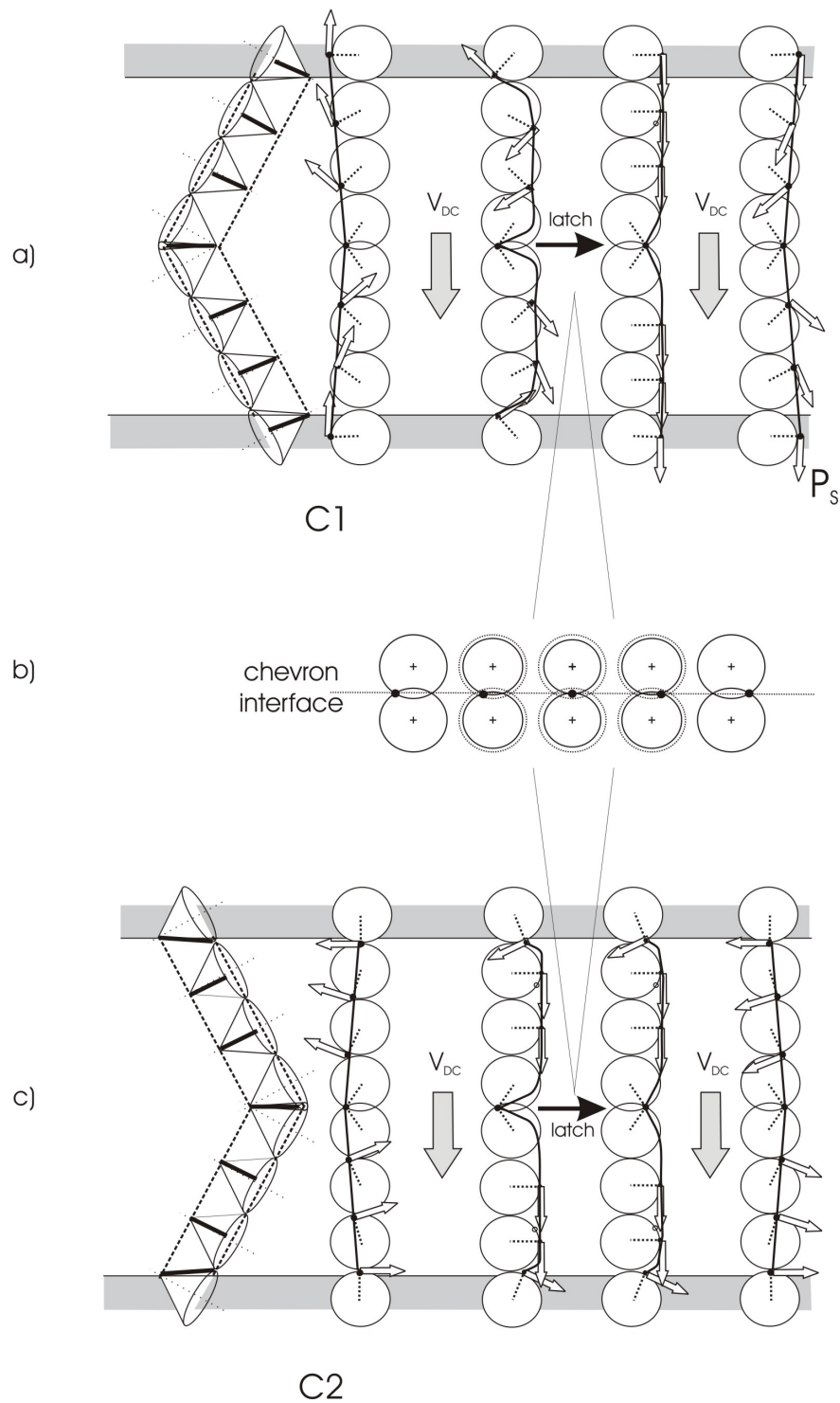
Unlike AC stabilisation, if the polarity of the applied field opposes the spontaneous polarisation reorientation occurs towards the opposite side of the cone, as shown in figure 11. The resulting high gradient close to the chevron interface will eventually be sufficient to cause the director to swap discontinuously from one allowed state to the other through the formation and movement of a domain wall. After removal of the field, the director relaxes back to a TDP but with the opposite sign to the original state. Crossing the energy barrier between the bistable states requires the director to move between the two allowed orientations at the chevron interface. This cannot occur by change in orientation ϕ_C alone and must involve compression of the smectic layers. Compressible continuum theories of the FLC phase, such as that of reference [16] have yet to be applied to latching at the chevron interface. Instead, simpler approaches have been taken, such as the empirical approach used in reference [24], or the Landau de Gennes [25] or numerical modelling [26] approaches. In the former approach, the transition is effectively instantaneous and discontinuous when the gradients of the **c**-director reach a critical torque T_0. One possibility [27] for the latching is that there is a momentary reduction of the smectic cone angle to $\theta_C = \delta_C$. Field induced changes of θ_C are termed "soft-mode", and are common close to the smectic A to smectic C transition temperature. At typical operating temperatures well below T_C, the soft-mode is energetically costly, and so the transition between the states will be highly first order. At this point, the **c**-director orientation at the chevron interface has solutions $\phi_C = \pm\pi/2$ in the two chevron halves and the director has a single orientation as shown in figure 11b. Figure 11a shows the latching transition for a high pre-tilt C1 chevron where the surface director also re-orients in response to the applied field. For the low tilt C2, chevron states, director reorientation at the surface is not essential if both states have equivalent director orientations as shown in figure 11c.

Usually, the coupling to the spontaneous polarisation is far stronger than the dielectric effect. Solving the torque equation (17) with $B_1=B_2=B_3$ and $B_{13}=\Delta\varepsilon=\boldsymbol{\partial\varepsilon}=0$ gives the response time τ:

$$\tau = \frac{\gamma_1 \sin^2 \theta_C}{P_S.\cos\delta_C.E} \qquad . \qquad (19)$$

Increasing the applied field reduces the latching time with a simple 1/E relationship. Typical values for FLC materials are $\gamma_1 \approx 0.25$ Pa.s and $\mathbf{P_S} = 50$ nCcm^{-2}, giving a predicted response time of 15ms for a |10V| signal in a 1.5μm cell. However, if the dielectric terms of equation (17) are important, the latching time will deviate from equation (19) as the dielectric torque opposes the ferroelectric latching torque. This effect is particularly noticeable if $|\mathbf{P_S}| / \partial e$ is low or the electric field E_z is high. In such instances, the dielectric terms reduce the rate of decrease of the latching time with increasing field strength until a minimum slot width is reached [28]. Above the so-called τV minimum, or τV_{min} the response slows rapidly with increasing field, ultimately diverging to infinity, at the field where the dielectric and ferroelectric torques balance. Numerical modelling shows that the τV minimum occurs at about 60 - 64% of the divergence field [29], given by:

$$V_{min} \approx 0.62 \frac{P_S d}{\varepsilon_0 \cos\delta_C} \left\{ \frac{1}{\left(\Delta\varepsilon \sin^2 \theta_C - \partial\varepsilon\right)^{2/3} - \left(\Delta\varepsilon \cos\theta_C \sin\theta_C \tan\delta_C\right)^{2/3}} \right\}^{3/2} \qquad (20)$$

Figure 11. Ferroelectric liquid crystal latching between "up" and "down" states. a) Latching in the C1 chevron state with high pre-tilt; b) potential model for latching at the chevron interface, c) Latching in the C2 chevron state with low pre-tilt.

with the minimum response time approximately:

$$\tau_{min} \approx \frac{\gamma_1 \sin^2 \theta_C \left(\Delta\varepsilon \sin^2 \theta_C - \partial\varepsilon \right)}{P_S^{\ 2}}$$

(21)

The shape of the τV curve depends on the dielectric, viscoelastic and tilt properties of the liquid crystal mixture, and the initial director profile dictated by the alignment geometry and degree of AC stabilisation. Accurate determination of the biaxial permittivities is a key step in understanding FLC material behaviour, and most importantly, for helping design improved S_C host and FLC materials. Before describing the measurement of the smectic C physical properties and biaxial order parameters in detail, the τVmin display mode is now reviewed.

2.4   Displays operating in the τV$_{min}$ mode.

Arguably, the most ambitious market targeted by any bistable display is large area HDTV. The requirement for very high contrast ratios, 60Hz frame rate and 16.8 million colours (256 grey-levels) would stretch passive matrix addressed FLC performance to the limit. In the mid-1990s, a collaborative programme between the UK Defence Research Agency (*DRA*, of which *RSRE* had become a part) and Sharp [30 - 33] developed 6" and 17" diagonal FLC displays aimed at meeting the HDTV specification. The approach chosen was to use the C2 chevron geometry, operating in the τV$_{min}$ mode that had previously been developed during under the UK *JOERS / Alvey* project [1,2].

The approach used to achieve the eight bits (256 levels) of grey was to combine two bits of spatial dither on the columns (weighted 1:2) with four temporal bits (weighted 1: 4 : 16 : 64). Even with the use of inter-laced lines, achieving a 60Hz frame rate on a 1920 × 1080 panel set the target line address time to be 15.4μs. Although the display was back-lit, and therefore usually operating whilst heated to about 30°C, this fast addressing speed was required for temperatures down to 15°C to

achieve the operating range 0°C to 60°C. This speed required ultra fast addressing schemes, uniform C2 alignment over large areas, and significant improvements to FLC materials.

There are a number of benefits proffered by C2 alignment. The spontaneous polarisation is parallel to the surface in both states, automatically reducing the tendency to form half-splayed states due to the effects of polar surfaces. Latching is not hindered by re-orientation at the surfaces, as shown in figure 11c: this helps achieve the fast speed, albeit with the loss of contrast on removal of the power as the display relaxes back to the quiescent state TDP. This is immaterial for televisions or computer monitors, since the optical contrast is retained through the application of the AC stabilising field inherent to any passive matrix addressing waveforms (due to the constantly applied data voltages). Of course, it is essential to ensure no remnant zigzag defects or areas of C1 are retained at the operating temperatures. This is done using surfaces with high anchoring energies, and matching the liquid crystal to the alignment layer to give the correct pre-tilt, as described in section 2.1. Maintaining the desired alignment requires the internal surfaces to be flat and that the colour filters and conductive bus-electrodes are planarised. The C2 alignment must be retained even when subjected to typical mechanical stresses, and this was done using regularly spaced adhesive polymer wall spacers [30, 34].

The principle of τV_{min} addressing is illustrated in figure 12. As for most passive matrix schemes, the panel is addressed row by row with a strobe signal (in this case, 0, $\pm V_s$) , with a data signal $\pm Vd$ applied synchronously to the columns. For bistable devices [34], the line will be latched into its appropriate image state after the strobe signal has moved onto the following lines. The basic τV_{min} scheme is designed to work close to the τV minimum: unlike conventional addressing, it is the lower voltage resultant $|V_s-V_d|$ that causes latching above the minimum, rather than the higher $|V_s+V_d|$ and the device operates with "inverted contrast". As can be seen from figure 11b, the gradient of the latching response is much steeper above the minimum as the response time diverges. This leads to an unusually high level of discrimination even for a small data voltage. The use of the inverted mode then allows a two-slot

mono-polar strobe pulse to be used (0, V_S), where the first slot of the data is synchronised with the 0V portion of the strobe. This leads to a pre-pulse in the select resultant of magnitude $|V_d|$ and with the same polarity as that required for latching, ensuring that the scheme is inherently fast. Contrast this with a bi-polar strobe pulse used more typically: with that scheme, the trailing latching pulse is always preceded by a high voltage that moves the director in the opposite direction to that required for latching, thereby inherently slowing the response. The $|V_s+V_d|$ portion of the τV_{min} mono-pulse scheme non-select resultant too is always preceded by a data pulse of the opposite polarity. This pulse acts to oppose any latching tendency of the non-select resultant, thereby further adding to the discrimination of the waveform.

Ignoring the elastic restoring torque and considering the electric terms of equation (17) only, the balance between dielectric and ferroelectric terms depends on the orientation about the cone ϕ_C. The ferroelectric torque is related to $+sin\phi_C$ and tends to a maximum at $\phi_C = \pi/2$. The dielectric torque, on the other hand, is dominated by the biaxiality and approximately related to $-(cos\phi_C \, sin\phi_C)$, which is maximum at $\phi_C = \pi/4$. In the C2 state, the initial director orientation lies between $\phi_C = \pi/2$ and $\pi/4$. At the early stage of the latching process, the dielectric term is high, and so the highest latching torque occurs for a relatively low voltage, where it is unopposed by the dielectric term. As the director reorients towards $\phi_C = \pi/2$, the opposing dielectric torque becomes less important, and so a higher voltage can be applied before the dielectric term begins to hinder reorientation. Figure 12b shows the evolution of the optimum latching torque as the director reorients, for the material SCE8. The mono-polar latching resultant follows the ideal shape for maximising the torque: the pre-pulse from the data in the first slot is small and so includes little dielectric hindrance. It "kicks" the director towards $\phi_C = \pi/2$, before $|V_s-V_d|$ is applied in the second slot. At that point, the higher voltage is then close to the optimum and latching is quickened. For the non-select resultant, the pre-pulse switches the director in the opposite direction, towards $\phi_C = \pi/4$. During the second slot, the higher voltage V_s+V_d is applied at a point where the dielectric term hinders latching to the greatest extent.

a) *graph showing Slot time τ / μs vs Peak Resultant Voltage / V*

b) *graph showing Voltage vs time / μs*
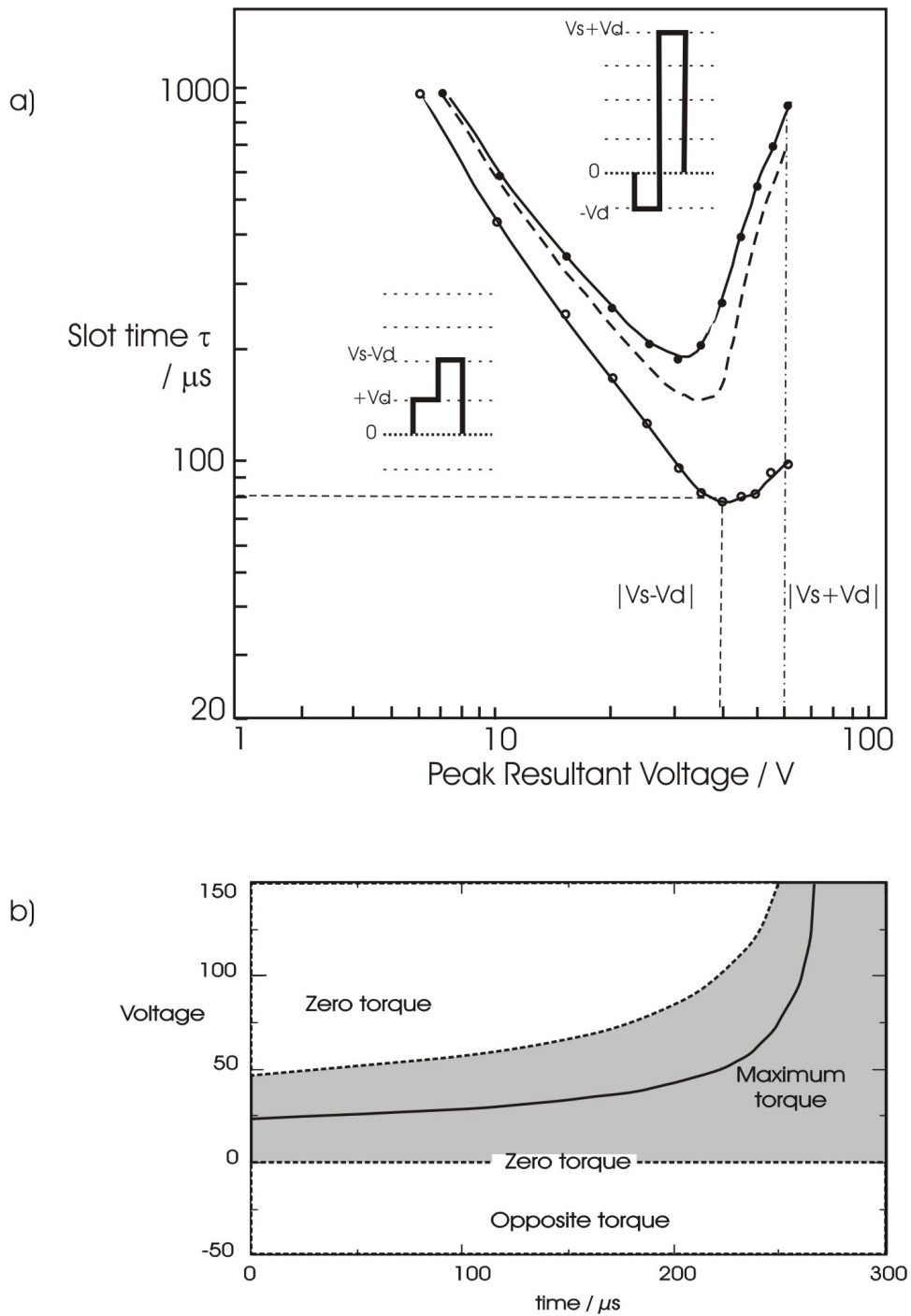
Figure 12. The principles of τVmin Addressing. a) SCE8 latching characteristic at 20°C in a 2μm cell for the mono-polar scheme resultants [1] (V_d = 10V); b) Temporal evolution of the optimum electric torque.
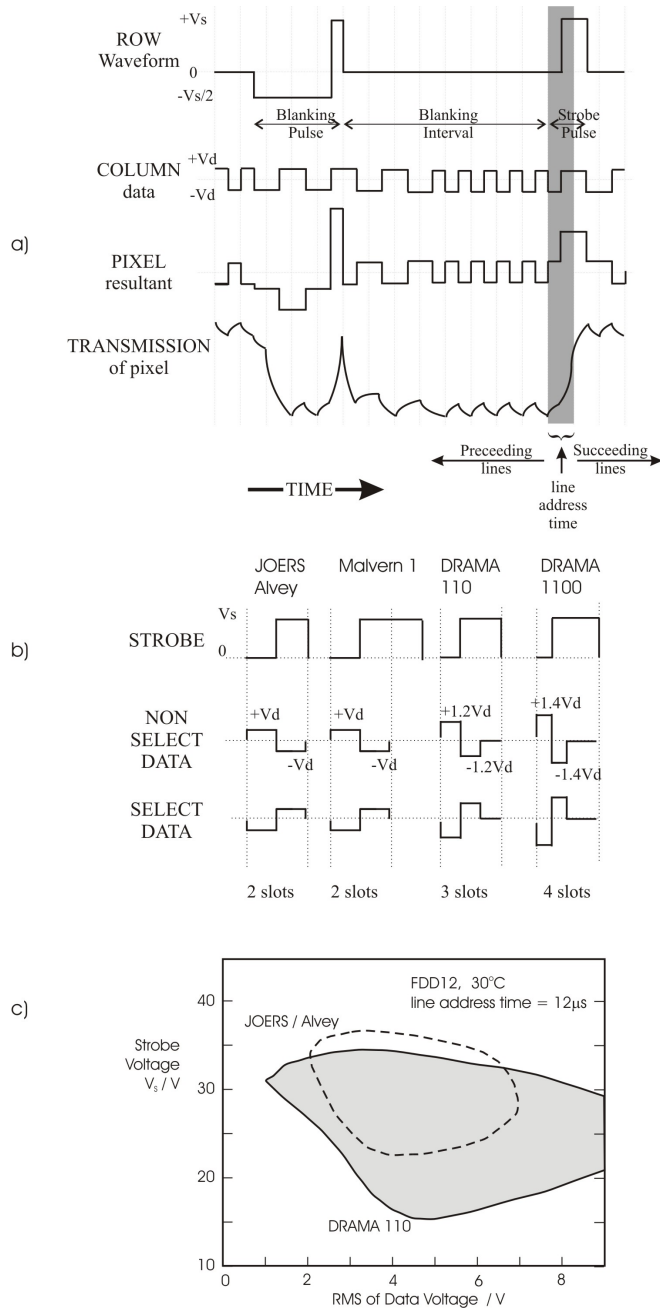
In practice, this simple scheme still could not achieve the high speeds required, and various addressing scheme improvement were required. An example of the full row waveform is also given in figure 13a. The scheme worked by blanking each row to one state first and then either latching to the opposite state if required, or leaving the pixel unchanged. Blanking to the black state gives the best possible contrast with only a minimal brightness reduction. Usually the blanking pulse is applied several lines ahead of the addressed line to avoid slowing the response to the select resultant. Of course, the interval must be kept reasonably short to reduce the unwanted reduction in brightness due to the period of black in successive white frames. Blanking and strobe pulses are mutually DC balanced whilst giving the maximum overlap of their respective operating windows. The large operating window of the τV_{min} mode means that the device can operate over a wide temperature range without changing the addressing parameters. Alternatively, the addressing scheme can be adapted to trade operating window for speed. The scheme shown in figure 13a uses a strobe pulse extended into the following line, the Malvern scheme [35]. The strobe increases the speed for both select and non-select resultants. This is because the data being applied in the extension is related to the following row and this data may act to slow the select and speed the non-select resultant, the discrimination of the two-wave forms is reduced. However, most of the discrimination of the pulse is dictated by the initial portion of the resultant, because of the manner in which the voltages for both maximum and minimum torque increase during the latching (see figure 12c). In the trailing row, the director for the select resultant is sufficiently reoriented to ensure that the high voltage at the end of the pulse aids latching regardless of the pixel pattern, whereas for the non-select resultant, the same high voltage is closer to the orientation where the dielectric term dominates. For this reason, extending the strobe into the following line is far more effective than extending it into the preceding row. Extending the strobe into the succeeding row(s) is a particularly powerful technique for global temperature compensation. Operation can be maintained across the temperature range without changing addressing parameters such as the slot time or addressing voltages by

simply adjusting the number of slots the strobe waveform is extended into the following rows.

Further optimisation to the addressing scheme used modification of the data waveforms to further enhance speed and operating window required to achieve HDTV operation. With DRA multiplexed addressing (DRAMA) [36] each line used 3 or 4 time slots, with zeros used in the third and fourth slot, figure 13b. This means that the discriminating portion of the data comprises pulses with a higher voltage than the RMS for the whole signal. This helps increase both speed and operating window, as shown in figure 13c, for the mixture FDD12 (see next section). The causes of this speed improvement are:

- The shape of the latching resultant more closely follows the maximum torque, since the pulse is terminated with one or two slots at V_s after the discriminating pulse at V_s-V_d.

- The scheme has no pixel pattern dependence associated with the row immediately ahead of the addressed row because both select and non-select signals are terminated with the same portion of zero volts.

The DRAMA data has a higher frequency, leading to a corresponding improvement in contrast ratio, although for a proportionately increased power consumption. SPICE modelling also shows that the power consumption (and any heating of the panel that it induces) is less pixel pattern dependent, and hence the panel temperature is more uniform.

ROW
Waveform
+Vs
0
-Vs/2

Blanking
Pulse

Blanking
Interval

Strobe
Pulse

COLUMN
data
+Vd
-Vd

a)

PIXEL
resultant

TRANSMISSION
of pixel

Preceeding
lines

Succeeding
lines

line
address
time

TIME

JOERS
Alvey

Malvern 1

DRAMA
110

DRAMA
1100

Vs
0

b)

STROBE

NON
SELECT
DATA

+Vd

+Vd

+1.2Vd

+1.4Vd

-Vd

-Vd

-1.2Vd

-1.4Vd

SELECT
DATA

2 slots

2 slots

3 slots

4 slots

c)

FDD12, 30°C
line address time = 12μs

40

JOERS / Alvey

Strobe
Voltage
V_s / V

30

20

DRAMA 110

10

0   2   4   6   8

RMS of Data Voltage / V

Figure 13. τV_{min} addressing a) Timing diagram for a row operating with the Malvern scheme [35]; b) Strobe and data waveforms for JOERS/Alvey, Malvern and DRA Multiplex Addressing (DRAMA) schemes; c) Mixture FDD12 τV_{min} operation with DRAMA 110 scheme [36] operating at 12μs per line.

3. Optical and Dielectric Biaxiality in Smectic C and FLC Liquid Crystals

3.1 Introduction

As has been seen, achieving the required ultra-high speed and operating window required the correct FLC alignment and addressing schemes to be designed. However, a key part to the optimisation procedure is the liquid crystal material design, and it is for this that George Gray's influence was strongest. Maximising the dielectric biaxiality is an important criterion for materials operating in the tV_{min} mode, both ensuring the maximum contrast through AC stabilisation, and reducing voltage and line-address time. This is considered in the following sections after studying the $S_C(*)$ refractive indices in more detail.

3.2 Biaxial $S_C(*)$ Refractive Indices

As with any liquid crystal material to be used in devices, ferroelectric liquid crystals are formed from multiple component mixtures to allow the properties to be optimised. Phase transition temperatures, dielectric, optical and visco-elastic constants are largely determined by an achiral host system, into which is added a small percentage (typically $2 - 5$ wt.%) of a chiral dopant to induce the ferroelectric spontaneous polarisation and helical pitch. Optimisation of physical properties such as the refractive indices and the electric permittivities for use in devices requires measurement methods to be defined, and the relationships between molecular structure, the order parameters and the physical properties obtained.

Liquid crystal refractive indices may be determined from critical angle measurements using an Abbé refractometer. Usually, homeotropic alignment is achieved using a monolayer of lecithin, to protect the soft glass of the high index prisms. For the uniaxial nematic and S_A phases, the ordinary refractive index, n_o, is obtained from the critical angle of the s-polarised light (in the surface plane) and the extraordinary index n_e from p-polarised light (normal to the surface plane). The situation is more complicated for the biaxial S_C and S_C* phases, as shown in figure 14. On cooling from a homeotropically oriented S_A, the smectic layers remain

parallel to the surface plane, but the director tilts, either randomly for the achiral S_C or in a helical fashion for the chiral S_C^*. The critical angle for a given polarisation is the lowest value from the sample. Thus, the ordinary and extraordinary indices are given by:

$$n_o = n_2 \; ;$$

$$n_e^2 = n_1^2 + (n_3^2 - n_1^2)cos^2\theta_c \; ; \tag{22}$$

for *s* and *p* polarised light respectively, where the tilted extraordinary index is corrected according to the approach of Yang and Sambles [37]. On the other hand if the c-director is uniformly arranged in the plane of light polarisation then the indices are:

$$n_o = n_1 \; ;$$

$$n_e = n_3 \; ; \tag{23}$$

for light polarised at the cone angle θ_C to *s* and *p* respectively (denoted *s'* and *p'* in figure 14). This geometry was originally [38] obtained using a combination of rubbed lecithin alignment and shearing for the achiral S_C host materials. More accurate values were obtained by Dunn [39] for a ferroelectric material by arranging for an in-plane electric field to be applied in the direction of light incidence. The temperature dependence of the refractive indices for the ferroelectric mixture SCE8 illuminated by the sodium line ($\lambda = 589.6$nm) are shown in figure 15. Also plotted is the mean refractive index $\bar{n} = \frac{1}{3}(n_e + 2n_0)$ for the uniaxial phases and $\frac{1}{3}(n_3 + n_2 + n_1)$ for the biaxial S_C^*, together with the extrapolated value from the uniaxial phases into the S_C^* phase using a linear 1/T dependence. The good agreement between the measured and extrapolated values adds confidence to the quality of the alignment achieved with the
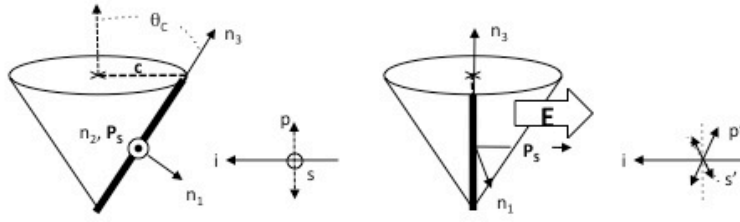
Figure 14. **FLC critical angle measurements for the c-director a) parallel and b) perpendicular to the incident light propagation direction, respectively.**

applied field. Substitution of the measured values for n_1 and n_3 into equation (22) allows the cone angle θ_C to be determined. The temperature dependence for θ_C found in this manner is shown in figure 16a, together with the layer tilt angle δ_C determined from X-ray rocking curves [39]. The temperature dependences are fitted using equations (2) and (3) but fixing both T_C and γ to be the same for both θ_C and δ_C thereby ensuring that δ_C/θ_C is temperature independent. The best fits to the equations gave $T_C = 59.3 \pm 0.3°C$, $v_o = v_l = 0.29 \pm 0.1$; $\theta_0 = 46.8 \pm 0.2°$ and $\delta_0 = 39.8 \pm 0.4°$, which gives $\delta_C/\theta_C = 0.85 \pm 0.02$, consistent with that found for other materials [6].

Figure 16b shows the temperature dependence for the uniaxial optical anisotropy $\Delta n = n_e - n_o$ for the uniaxial N and S_A phases and $n_3 - n_1$ for the biaxial S_C*, and the optical biaxiality $\partial n = n_2 - n_1$. Clearly, the optical biaxiality is small $\partial n \approx 0.001$, and approaches the experimental uncertainty. However, it should be noted that, unlike the uniaxial phases, shearing of the sample led to movement of the ordinary critical angle demarcation line, which is indicative of a finite, though small, optical biaxiality as the ordinary index fluctuates between n_1 and n_2.
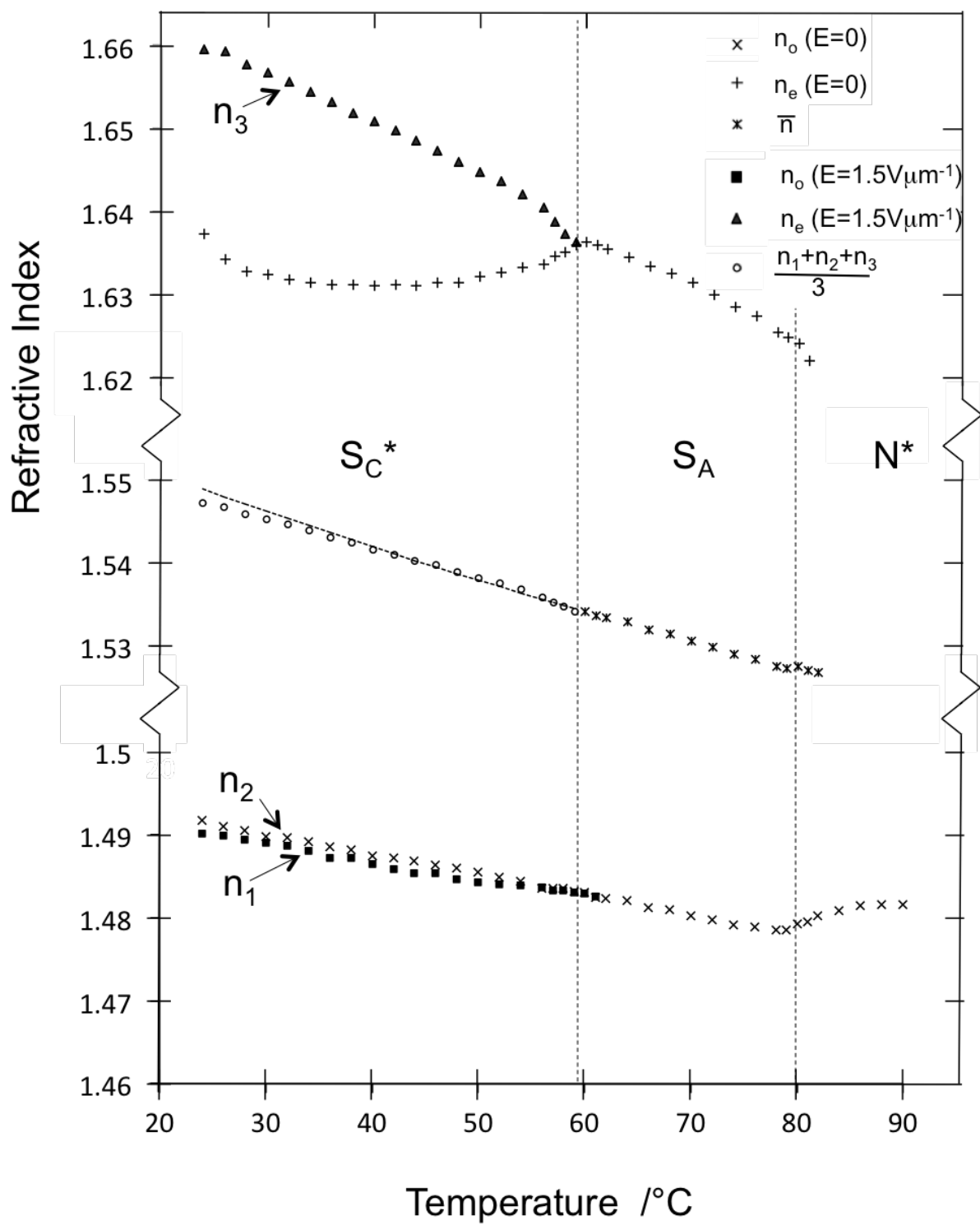
Figure 15. Refractive indices for the Ferroelectric Liquid Crystal SCE8 (589.6nm).

a)   b)
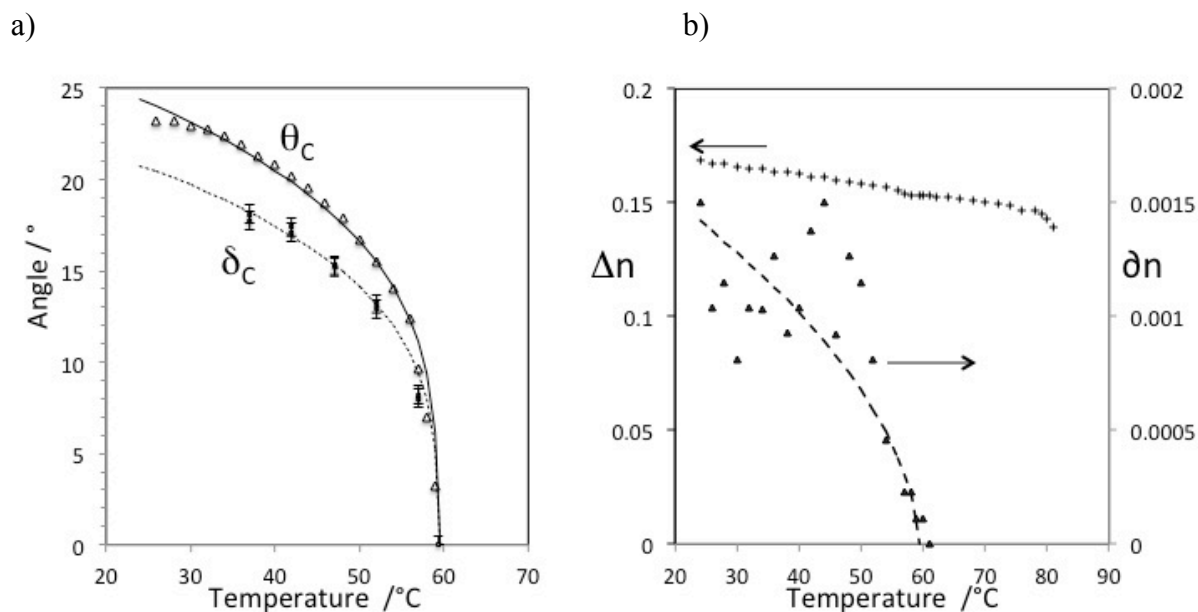
Figure 16. **a) Temperature dependence of the SCE8 cone angle θ_C calculated from refractive index data, and layer tilt angle δ_C from X-ray rocking curves; b) Birefringence and optical biaxiality for SCE8.**

3.2   *Biaxial $S_C(*)$ Dielectric constants*

As explained previously, the biaxial nature of the S_C phase had been realised from the outset, [18] but measurements showed that the optical biaxiality is negligible [19] and it had been assumed that the dielectric biaxiality was also insignificant. It was Roy Sambles who first realised that the AC stabilising effect of negative $\Delta\varepsilon$ $S_C(*)$ mixtures in the chevron geometry had to have a significant dielectric biaxiality, in discussions with Peter Raynes and Frank Leslie. I remember Frank rushing to tell me at RSRE since I had already undertaken the challenge of measuring the dielectric biaxiality for S_C and S_C* Phases. Roy Sambles's idea was then proven using a two-frequency S_C host based on a phenyl pyrimidine host that gave a

higher degree of AC stabilisation at frequencies where $\Delta\varepsilon \approx 0$ than for those where $\Delta\varepsilon < 0$ [20].

If orthorhombic symmetry of the $S_C(*)$ phase is assumed, then at least three permittivity measurements are required to determine the principal permittivity components ε_1, ε_2 and ε_3, providing that the cone angle θ_C is known. The permittivity for a uniform structure is [21]:

$$\begin{aligned}
\varepsilon &= \varepsilon_1(cos\delta_C cos\theta_C sin\phi_C + sin\delta_C sin\theta_C)^2 + \varepsilon_2 cos^2\delta_C cos^2\phi_C \\
&\quad + \varepsilon_3(cos\delta_C sin\theta_C sin\phi_C + sin\delta_C cos\theta_C)^2 \\
&= \varepsilon_1 + \Delta\varepsilon. sin^2\omega + \partial\varepsilon. cos^2\delta_C cos^2\phi_C \qquad ; \qquad (24)
\end{aligned}$$

where ω is the out-of-plane tilt of the director given by:

$$\omega = sin^{-1}(cos\delta_C sin\theta_C sin\phi_C - sin\delta_C cos\theta_C) \qquad . \qquad (25)$$

Assuming the measurement cell has uniform alignment, where δ_C and ϕ_C are constant then the homeotropic ε_h and planar homogenous permittivities ε_p are:

$$\varepsilon_h = \varepsilon_1 sin^2\theta_C + \varepsilon_3 cos^2\theta_C = \varepsilon_3 - \Delta\varepsilon. sin^2\theta_C \qquad , \qquad (26)$$

and

$$\varepsilon_p = \varepsilon_2 - \partial\varepsilon \frac{sin^2\delta_C}{tan^2\theta_C} \qquad , \qquad (27)$$

respectively. The third permittivity value has been provided by different methods. In the original work [21], the mean permittivity $\bar{\varepsilon}$ is extrapolated linearly in 1/T from the isotropic phase and uniaxial nematic and smectic A phases:

$$\bar{\varepsilon} = \frac{\varepsilon_{||} + 2\varepsilon_\perp}{3} = 1 + \frac{NhF}{\varepsilon_0}\left[\bar{\alpha} + \frac{F\mu^2}{3k_BT}\right] \qquad , \qquad (28)$$

where N is the number density, $\bar{\alpha}$ the mean polarisability, ε_0 the free-space permittivity and k_B the Boltzmann constant. h and F are the usual Debye cavity field factors:

$$h = \frac{3\varepsilon}{2\varepsilon+1} \quad ; \quad F = \frac{1}{1-\alpha f} \quad ; \quad f = \frac{2N}{3\varepsilon_0}\left(\frac{\varepsilon-1}{2\varepsilon+1}\right) \qquad (29)$$

with α and ε the polarisability and permittivity of the spherical cavity surrounding the molecule, Below the $S_C(*)$ phase transition, the mean permittivity is given by:

$$\bar{\varepsilon} = \frac{\varepsilon_1 + \varepsilon_2 + \varepsilon_3}{3} \qquad , \qquad (30)$$

which gives the three permittivities on simultaneous solution with equations (26) and (27):

$$\varepsilon_3 = \frac{\left(3\bar{\varepsilon}sin^2\theta_C - \varepsilon_h\right)\left(tan^2\theta_C - sin^2\delta_C\right) - \varepsilon_p tan^2\theta_C sin^2\theta_C + \varepsilon_h sin^2\delta_C}{\left(sin^2\theta_C - cos^2\theta_C\right)\left(tan^2\theta_C - sin^2\delta_C\right) + cos^2\theta_C sin^2\delta_C}$$

$$\varepsilon_1 = \frac{\varepsilon_h - \varepsilon_3 cos^2 \vartheta_C}{sin^2 \theta_C}$$

$$\varepsilon_2 = 3\bar{\varepsilon} - \varepsilon_3 - \varepsilon_1 \tag{31}$$

Results for the temperature dependent permittivities of the racemic ferroelectric mixture SCE8 (R) are shown in figure 17. Use of achiral mixtures avoids complications of poor alignment due to the effect of helicity in the N* and S_C* phases, and surface polarity effects in the S_C*. Importantly, the large contribution to the measured permittivity from the Goldstone and Soft mode switching effects restricts accurate measurement of the dielectric constant to high frequencies, where electrode resistance effects also become important. However, the large errors observed in the values for the biaxial components ε_1, ε_2 and ε_3 are dominated by uncertainties of $\bar{\varepsilon}$.

A second method [38] of deriving the permittivities used DC field switching of the ferroelectric polarisation for a mixture chemically similar to SCE8 and based on the Phenyl 2-fluoro biphenyl carboxylates. The mixture was arranged to have a low spontaneous polarisation of $10nCcm^{-2}$ at 35°C and was studied in a 50μm cell to reduce electrode effects. The DC field reorients the director towards the orientation $\phi_C = 0$ or π. Substitution of this condition into equation (24) gives:

$$\varepsilon_{DC} = \varepsilon_2 + (\Delta\varepsilon.cos^2\theta_C - \partial\varepsilon)sin^2\delta_C \qquad , \tag{32}$$

where the subscripted DC indicates an applied electric field that is sufficiently high to cause complete reorientation of the director but without disruption of the layers. Simultaneous solution of equations (26), (27) and (32) gives the results shown in figure 18, where the results are compared with those made by extrapolating $\bar{\varepsilon}$. Note, there is a slight decrease of the permittivity with increasing field: this is caused by the quenching effect of the DC field on the Goldstone mode fluctuations still affecting the results even at 100kHz.

A similar method [40] used a thick sample with a helical structure. Ignoring the effect of the chevron interface, the permittivity is approximately:
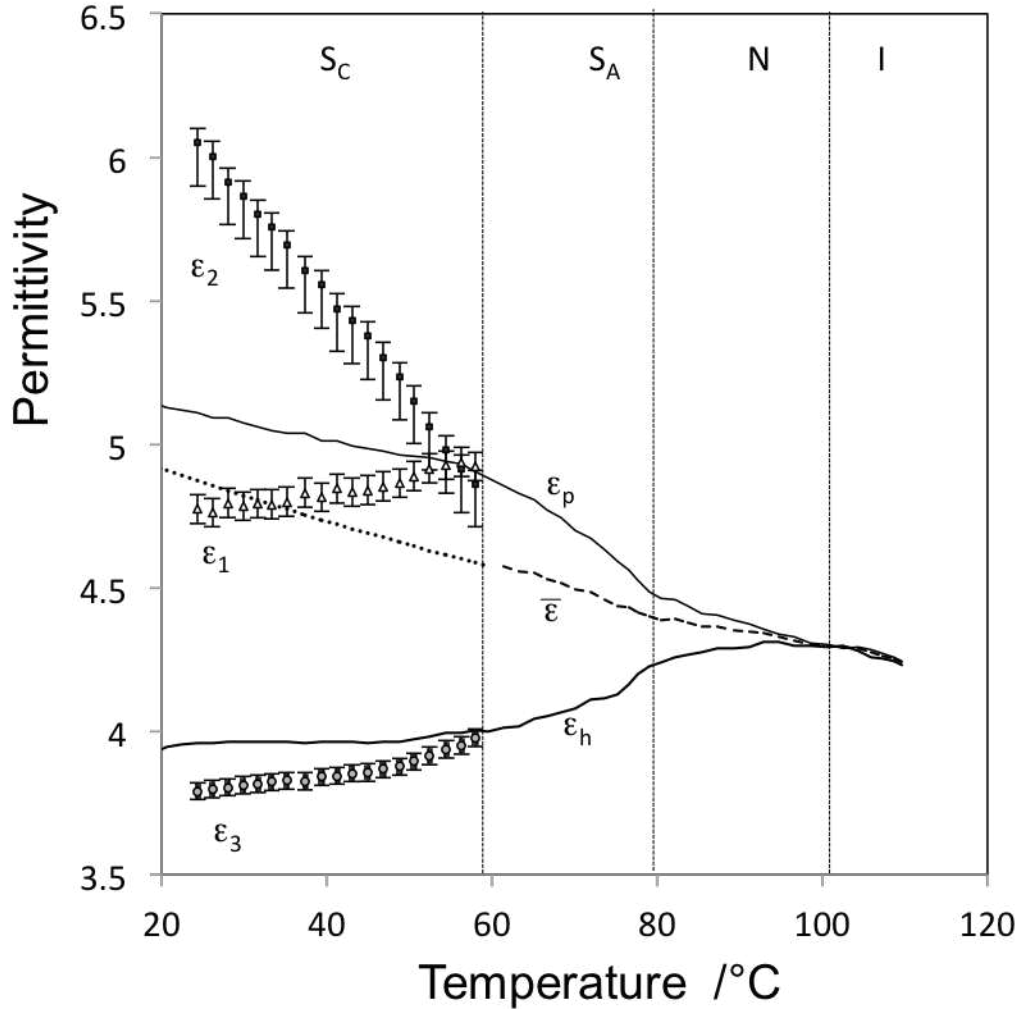
Figure 17. **Temperature dependence of the biaxial permittivities for the racemic Ferroelectric Liquid Crystal SCE 8. The solid lines show the measured values for planar homogenous ε_p and homeotropic ε_h cells. The mean permittivity $\bar{\varepsilon}$ is shown as a dashed line, together with the S_C values extrapolated according to equation (28), as a dotted line.**
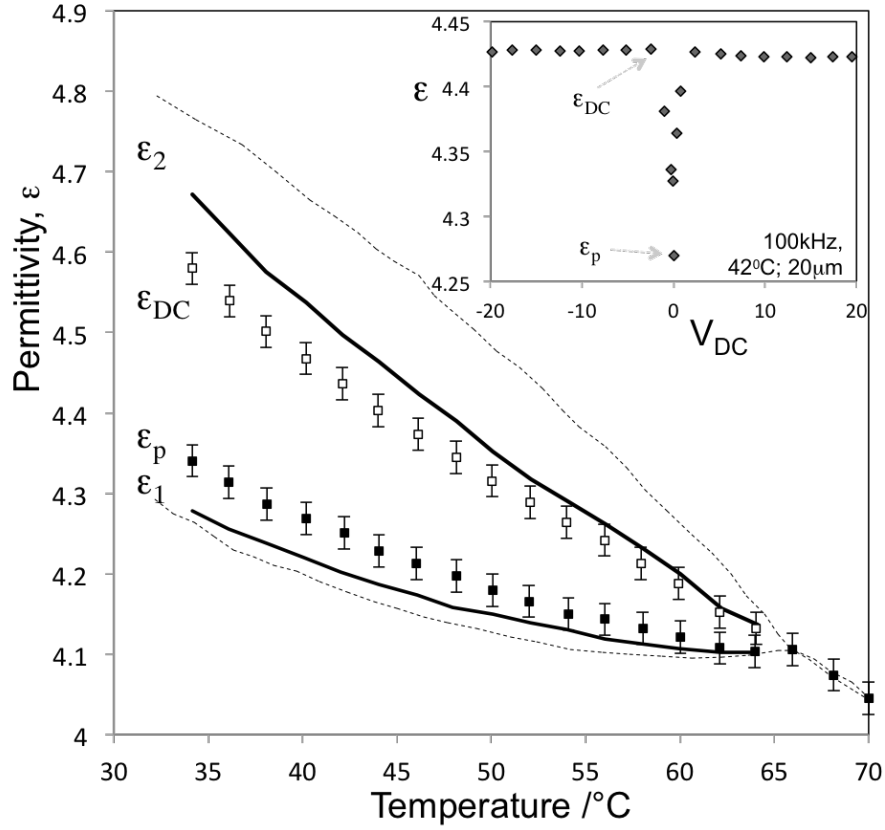
Figure 18. **Perpendicular permittivities for a FLC mixture similar in composition to SCE8 measured using DC switching. Solid lines show the values obtained from extrapolation of the mean permittivity. Inset is an example of the FLC permittivity behaviour with applied DC voltage.**

$$\varepsilon_{helix} = \frac{1}{2}\cos^2\delta_c(\varepsilon_1\cos^2\theta_c + \varepsilon_3\sin^2\theta_c + \varepsilon_2) + \sin^2\delta_c(\varepsilon_1\sin^2\theta_c + \varepsilon_3\cos^2\theta_c) \qquad (33)$$

The high frequency permittivities can then be found from equations (26), (31) and (33). A comparison of the permittivities made using each of these approaches has yet to be done using the same materials, though the values of [21, 38, 40] are similar in magnitude.

The most accurate method for determining the permittivities so far is that reported by Brown and Jones [41] who used the AC stabilising effect of the field applied to determine the permittivity, fitting of the resultant $\varepsilon(V)$ curve through numerical solution of equation (11). The starting configuration for ε_p used a triangular director profile [17], and again it was assumed that the field was insufficient to cause change in θ_C, δ_C or the layer structure. This latter assumption was justified by restricting the voltages to those below the formation of "needle" defects in the sample, and by checking that the permittivity was free from hysteresis with reducing field. For the fits, strong anchoring at the chevron interface was assumed, and the elastic constants B_3 and B_{13} were assumed as zero.

Figure 19 compares the SCE8 1kHz results obtained from the AC field method with those determined from the $\bar{\varepsilon}(T)$ extrapolation. Although there is excellent agreement between the methods for ε_3 and $\bar{\varepsilon}$, there is a large discrepancy between the values of the perpendicular components found with the two methods: at 24C ε_1 is 5.1 compared to 4.8 by extrapolation, and ε_2 is 5.6 compared to 6.0 by extrapolation. This is ascribed to two systematic errors with the $\bar{\varepsilon}(T)$ extrapolation. Firstly, the correction for the TDP structure of the quiescent state [21] leads to ε_1 being 4% ($\approx$0.2) higher and ε_2 being 2% lower (0.1) than would be achieved with a uniform director profile of equation (27). The remaining largest systematic error is associated with the extrapolation itself, and the poor linearity through the N to S_A phase transition. Interestingly, the ferroelectric mixture that is also based on a fluorinated biphenyl carboxylate gives similar magnitude of biaxiality $\partial\varepsilon$ to that of SCE8, though measured through the DC extrapolation.
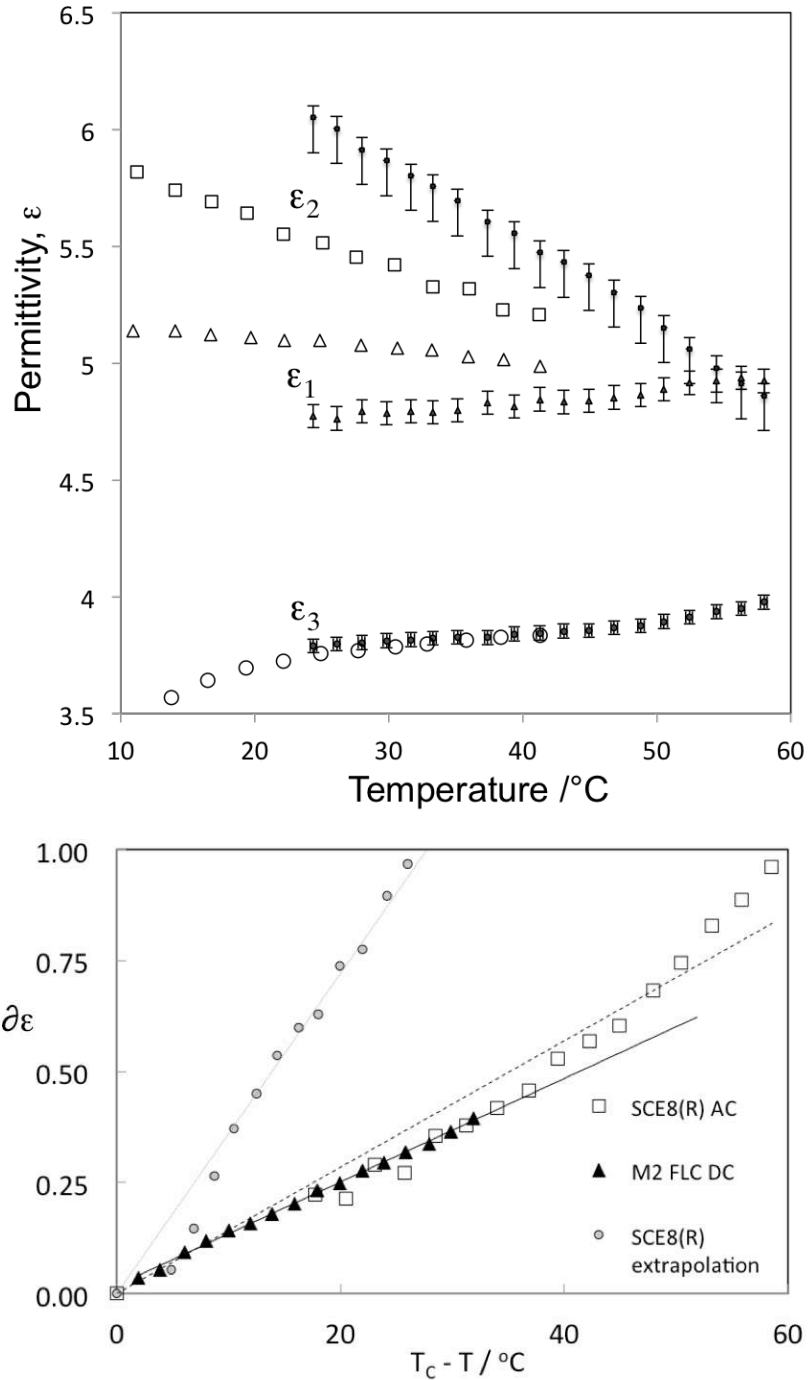
Figure 19. Temperature dependence SCE8 S_C permittivities at 1kHz. a) The biaxial electric permittivities determined through fitting the AC dependence [41] (open symbols) compared to the values obtained by extrapolation (closed symbols); b) Comparison of the dielectric biaxiality $\partial\varepsilon$ for SCE8 (R) measured through fitting $\varepsilon(V_{AC})$ and using the extrapolated $\bar{\varepsilon}$. Also shown are the values for the FLC mixture M2 determined using the high field permittivity ε_{DC}

4.   Biaxial Order and measurement of the C-order parameter

Considering the second rank elements of the order parameter tensor only, a biaxial system composed of biaxial molecules still requires four parameters, given by [42, 43]:

$$S = \frac{1}{2}\langle 3\cos^2\xi - 1\rangle \tag{33}$$

$$D = \frac{3}{2}\langle 3\sin^2\xi \cos 2\zeta\rangle \tag{34}$$

$$P = \frac{3}{2}\langle 3\sin^2\xi \cos 2\eta\rangle \tag{35}$$

$$C = \frac{3}{2}\langle(1+\cos^2\xi)\cos 2\zeta \cos 2\eta - 2\cos\xi \sin 2\zeta \sin 2\eta\rangle \tag{36}$$

where ξ, ζ and η are the molecular Euler angles, shown in figure 20. S, of course represents the distribution of molecular long axes with respect to the **n** director. If the molecule is biaxial, then order of a short molecular axis with respect to the **n** director is quantified by D. For example, a negative $\Delta\varepsilon$ material has a perpendicular dipole ($\mu_\perp$) and is inherently biaxial. S-like fluctuations of ξ may occur with this dipole either in the plane of the fluctuation, or normal to it. The phase still has uniaxial cylindrical symmetry, since the fluctuations of ξ occur with equal probability in all orientations about the director η. As the temperature is lowered and fluctuations of the long molecular axis reduce, such that S tends towards 1, and D towards zero. Usually, the onset of smectic order means that S is high for $S_C(*)$ and D can be ignored safely.

The onset of director tilt in the $S_C(*)$ phase necessitates biaxiality and the phase has a single symmetry C_2 axis (and a mirror plane for the achiral material). For simplicity, we shall assume orthorhombic symmetry, so that the **n** director remains well defined, and S and D retain continuity from the uniaxial phases. The additional order parameters P and C then represent order of the long and short molecular axes

with respect to the C_2 symmetry axis of the phase, which we shall term the **m** director. P quantifies anisotropic S-like fluctuations that may be larger parallel to **m** than perpendicular to it. Fluctuations of ξ die down as the temperature is lowered and S increases. This is accompanied by a reduction of the P order parameter, which vanishes at absolute zero. As for the D order parameter, C represents hindered rotation of the director but quantifies the degree of ordering of the short molecular axis with respect to **m**. Unlike D and P, C increases with reducing temperature, tending towards C = 3 at absolute zero, where S is unity. For high S, C can be approximated as:

$$C = 3\langle \cos 2\eta \rangle \qquad\qquad (37)$$

a form that is often used to represent the degree of hindered rotation about the **n**-director for biaxial phases.
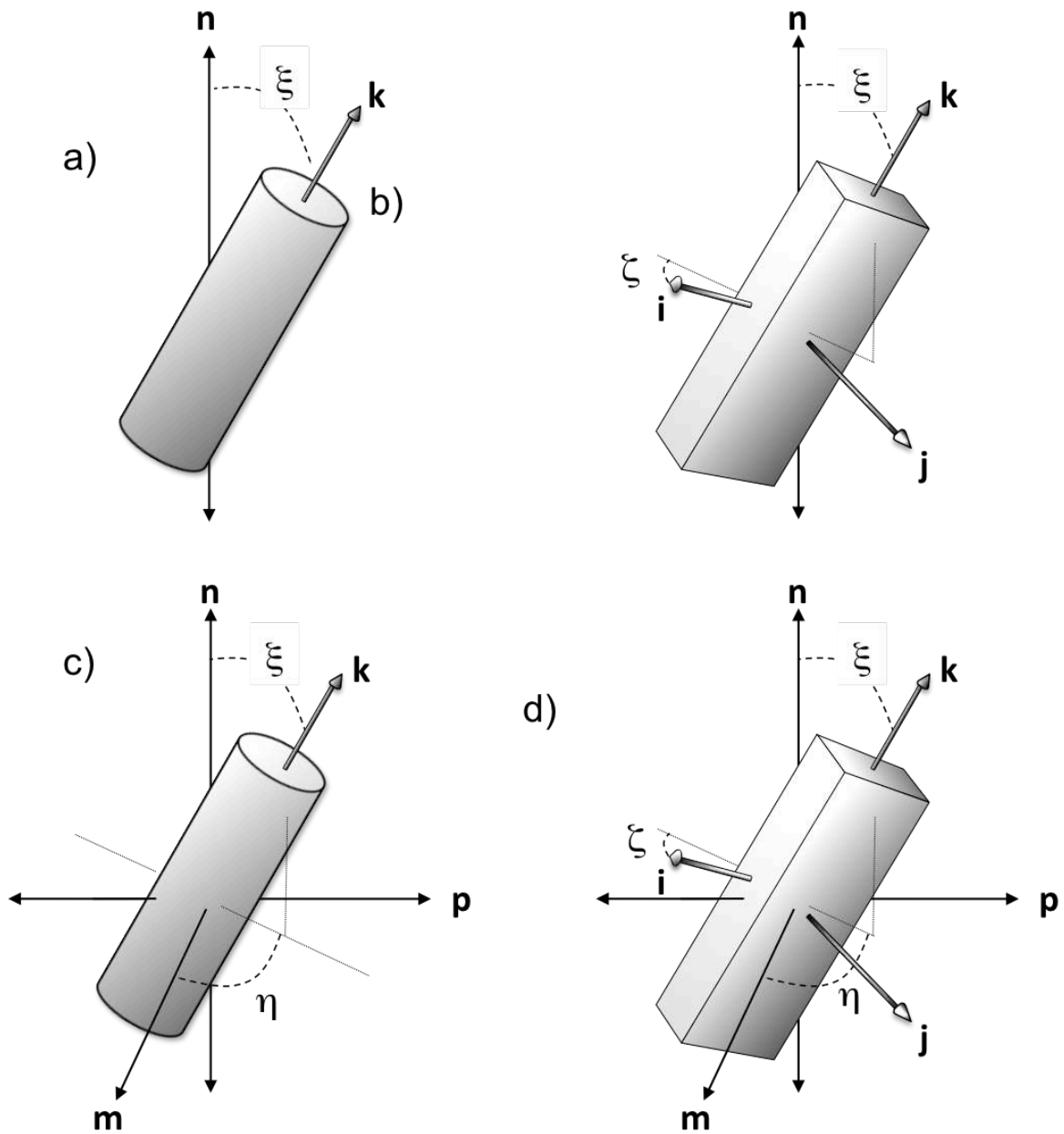
Figure 20. Molecular fluctuations in uniaxial and biaxial phases. Fluctuation of a) the long and b) short molecular axes from the n director, quantified by S and D, respectively. Fluctuation of a) the long and b) short molecular axes from the m director (parallel to the C_2 symmetry axis), quantified by P and C, respectively

The biaxial permittivities are given by [34]:

$$\varepsilon_1 - 1$$

$$= \frac{NhF}{\varepsilon_0} \left\{ \begin{array}{c} \bar{\alpha} - \frac{1}{3}\Delta\alpha(S-P) - \frac{1}{6}\partial\alpha(D-C) \\ + \frac{Fg_1}{6k_BT}[\mu_1^2(2+S-P-D+C) + \mu_2^2(2+S-P+D-C) + 2\mu_3^2(1-S+P)] \end{array} \right\}$$

$$\varepsilon_2 - 1$$

$$= \frac{NhF}{\varepsilon_0} \left\{ \begin{array}{c} \bar{\alpha} - \frac{1}{3}\Delta\alpha(S+P) - \frac{1}{6}\partial\alpha(D+C) \\ + \frac{Fg_2}{6k_BT}[\mu_1^2(2+S+P-D-C) + \mu_2^2(2+S+P+D+C) + 2\mu_3^2(1-S-P)] \end{array} \right\}$$

$$\varepsilon_3 - 1 = \frac{NhF}{\varepsilon_0} \left\{ \begin{array}{c} \bar{\alpha} + \frac{2}{3}\Delta\alpha S + \frac{1}{3}\partial\alpha D \\ + \frac{Fg_3}{3k_BT}[\mu_1^2(1-S+D) + \mu_2^2(1-S-D) + \mu_3^2(1+2S)] \end{array} \right\} \qquad (38)$$

where the g1, g2, an g3 are the Kirkwood dipole correlation factors. Given that the mean permittivity is linear across the various phase transitions (including the S_A-S_C(*) when the direct methods of measuring S_C(*) biaxial permittivities are deployed) then dipole correlation are assumed to be irrelevant, so that the average permittivity, $\bar{\varepsilon}$ is given by:

$$\bar{\varepsilon} - 1 = \frac{NhF^2}{\varepsilon_0 k_B T}\mu^2 \qquad (39)$$

Optical frequencies are too high to induce reorientation of the molecular dipoles, and so the refractive indices are related to the polarisabilities only:

$$n_1^2 = 1 + \frac{NhF}{\varepsilon_0}\left\{ \bar{\alpha} - \frac{1}{3}\Delta\alpha(S-P) + \frac{1}{6}\partial\alpha(D-C) \right\} \qquad (40)$$

$$n_2^2 = 1 + \frac{NhF}{\varepsilon_0}\left\{\overline{\alpha} - \frac{1}{3}\Delta\alpha(S+P) + \frac{1}{6}\partial\alpha(D+C)\right\} \tag{41}$$

$$n_3^2 = 1 + \frac{NhF}{\varepsilon_0}\left\{\overline{\alpha} + \frac{2}{3}\Delta\alpha S - \frac{1}{3}\partial\alpha D\right\} \tag{42}$$

For the uniaxial phases, where P and C = 0, then

$$n_o^2 = n_1^2 = n_2^2 = 1 + \frac{NhF}{\varepsilon_0}\left\{\overline{\alpha} - \frac{1}{3}\Delta\alpha S + \frac{1}{6}\partial\alpha D\right\} \tag{43}$$

$$n_e^2 = n_3^2 = 1 + \frac{NhF}{\varepsilon_0}\left\{\overline{\alpha} + \frac{2}{3}\Delta\alpha S - \frac{1}{3}\partial\alpha D\right\} \tag{44}$$

from which the mean of the indices squared is:

$$\overline{n^2} - 1 = \frac{1}{3}\left(n_1^2 + n_2^2 + n_3^2\right) = \frac{1}{3}\left(n_e^2 + 2n_o^2\right) = \frac{NhF}{\varepsilon_0}\overline{\alpha}. \tag{45}$$

This allows the familiar Vuks and Haller relationships to be found:

$$\frac{n_e^2 - n_o^2}{\overline{n^2} - 1} = \frac{\Delta\alpha S - \partial\alpha D}{\overline{\alpha}} \approx \frac{\Delta\alpha}{\overline{\alpha}}S = \left(1 - \frac{T}{T_{NI}}\right)^m \tag{46}$$

The equivalent expressions for the optical biaxiality are:

$$\frac{n_2^2 - n_1^2}{\overline{n^2} - 1} = \frac{\partial\alpha C - 2\Delta\alpha P}{3\overline{\alpha}} \approx \frac{\partial\alpha}{\overline{\alpha}}C = \left(1 - \frac{T}{T_C}\right)^{m'} \tag{47}$$

where the assumption that the P $\ll$ C has been made. Fits to equations (46) and (47) allow the order parameters S and C to be measured, together with the molecular

quantities $\Delta\alpha/\bar{\alpha}$ and $\partial\alpha/\bar{\alpha}$. Using the SCE8 refractive indices of figure 15 gives $\frac{\Delta\alpha}{\bar{\alpha}} = 0.47\pm0.02$ and $\partial\alpha/\bar{\alpha} = 0.011\pm0.005$, and the calculated order parameters are shown in figure 21. Small increases of S order were observed at both the N-S_A and S_A-S_C phase transitions, leading to a room temperature value of S 0.8, which is typical of smectic liquid crystals. The magnitude of the biaxial order parameter is high, and is fit by the expression:

$$C = C_0 \sin^2 \theta_C \qquad (48)$$

for which the best fit for SCE8 is has $C_0 = 1.7$. Given the results of [21] taken on a variety of S_C hosts from phenyl-pyrimidines to fluorinated terphenyls, together with the results herein, it seems likely that this magnitude of biaxial order is typical.

Estimates for the order parameters can also be made using the permittivities. We shall assume that a perfectly ordered smectic C or C* has the perpendicular dipole parallel to the phases C_2 symmetry axis, ($\mu_2 = \mu_\perp$; $\mu_1 = 0$ and $\mu_3 = \mu_{||}$) then:

$$\varepsilon_\perp = \frac{\varepsilon_2 + \varepsilon_1}{2} = 1 + \frac{NhF}{\varepsilon_0}\left\{\bar{\alpha} - \frac{1}{3}\Delta\alpha S - \frac{1}{6}\partial\alpha D + \frac{F}{6k_BT}\left[\mu_\perp^2(2 + S + D) + 2\mu_{||}^2(1 - S)\right]\right\} \quad (49)$$

and

$$\frac{\varepsilon_{||} - \varepsilon_\perp - (n_e^2 - n_o^2)}{\bar{\varepsilon} - 1} = \frac{1}{2\mu^2}\left\{2\mu_{||}^2 S - \mu_\perp^2(S + D)\right\} \approx \frac{2\mu_{||}^2 - \mu_\perp^2}{2\mu^2}S \qquad (50)$$

$$\frac{\partial\varepsilon - \partial n^2}{\varepsilon_\perp - n_o^2} = \frac{1}{3\mu_\perp^2}\left\{\mu_\perp^2(P + C) - 2\mu_{||}^2 P\right\} \approx \frac{1}{3}C \qquad (51)$$

Equation (50) can give a reasonable estimate for S for strongly negative ($\mu_\perp \approx \mu$) or positive ($\mu_{||} \approx \mu$) materials [44], but SCE8 is only weakly negative, and S cannot be predicted accurately (even if the dipole moments are known). However, more success is possible for the prediction of the C order parameter using equation (51), as also

shown by the results in figure 21, where there is excellent agreement between the biaxial order found using the permittivities and that found from the refractive indices, which is a rather gratifying result.
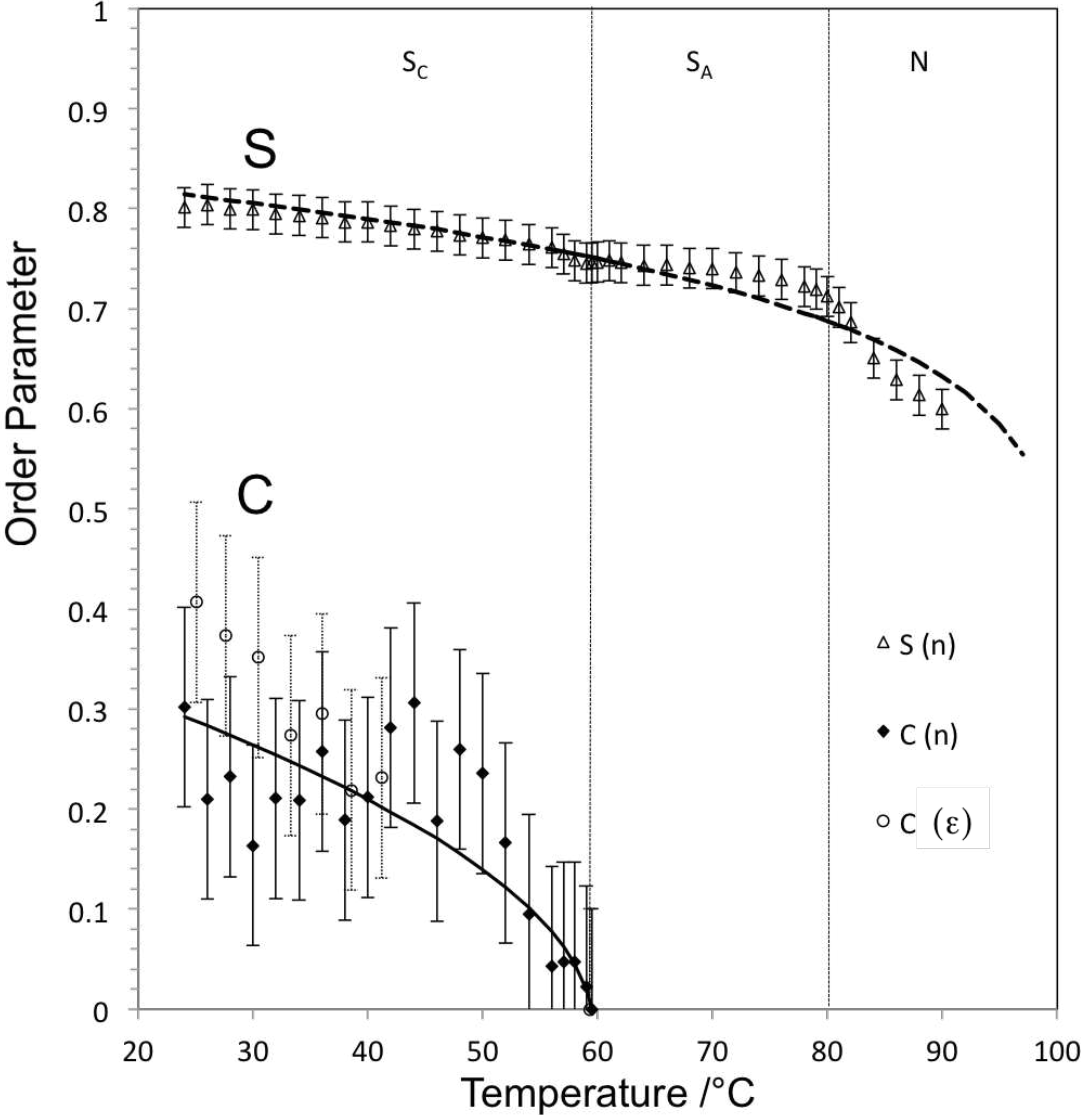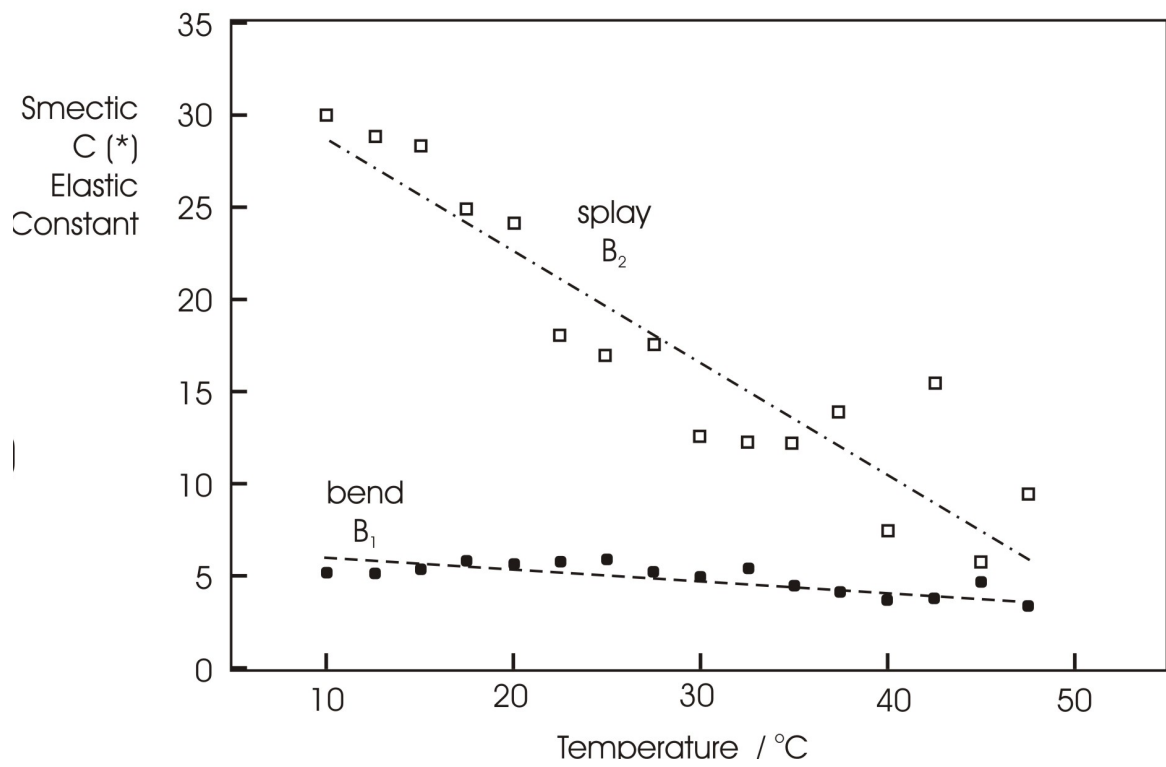

Figure 21. **Temperature dependence of the S and C order parameters for SCE8 (R). The dashed lines represent the fit to the Haller equation (45) for S, and the full line is the fit of the biaxial order parameter C to equation 49.**

54

5.   Implications for FLC material design

In addition to providing accurate values for the biaxial permittivities, the $\varepsilon(V)$ fitting procedure deployed by Brown and Jones [41] provides measurements for the S_C **c**-director bend and splay elastic constants B_1 and B_2 (where $B_3 = B_{13} = 0$ was assumed). The temperature dependence of the elastic constant for SCE8(R) is shown in Figure 22. Indeed, it was these values that were used earlier for calculating the theoretical AC field dependence of the optical extinction angles as a function of temperature shown in figure 10a.

Figure 23 shows experimental results for the latching characteristic of the FLC mixture SCE8 in the C2 geometry of figure 4a, together with a numerical fit to equation (11). The viscosity γ_1 and critical chevron latching torque T_0 were free variables for the fit, B_3 and B_{13} were fixed at estimates based on a comparison made with nematic elastic constants, and measured quantities were used for $\mathbf{P_S}$, θ_C, δ_C, $\Delta\varepsilon$, $\partial\varepsilon$, B_1 and B_2. The values of $\partial\varepsilon$, B_1 and B_2 were allowed to vary within the experimental errors of the measurements [27]. Figure 23b shows the effect of varying the elastic constants B_1 and B_2 on the bistable latching characteristic. For operation in the τVmin mode, the results show that the ideal material has the following characteristics:

- $\Delta\varepsilon$ as close to zero as possible (even slightly positive);
- $\partial\varepsilon$ as high as possible, to reduce both τVmin and increase the AC stabilisation effect;
- B_1 high, since it has a strong effect on reducing τVmin, in particular for achieving a fast response speed. This is the most important of the elastic constants to optimise;
- B_2 should also be high, since this increases the gradient of the latching characteristic above V_{min}, and improves display multiplexibility.

Figure 22. ***Temperature dependences of the c-bend (B₁) and c-splay (B₂) elastic constants obtained in the fitting procedure for the AC field.***

a)

b)
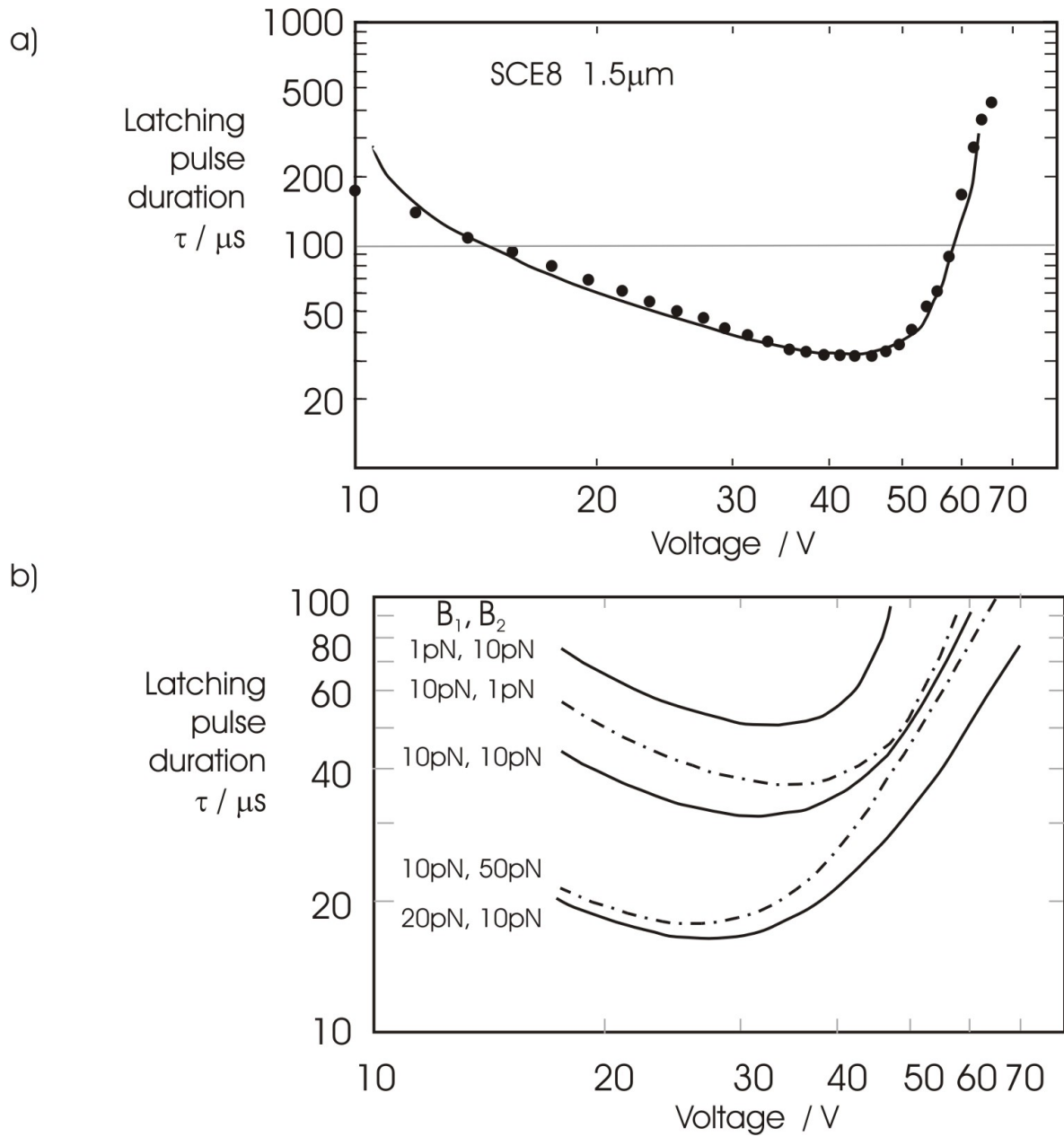
Figure 23. The τV minimum FLC latching response. a) Comparison of theory and experiment for a 1.5mm SCE8 cell in the C2 geometry. The line shows the best numeric fit to equation (47). The fitting parameters are: $\partial\varepsilon$ = +0.5, B_1 = 1pN, B_2 = 5pN, γ_1=30cP and the critical latching torque T_0=0.6×10^{-4}N/m. Independent measured properties include P_S = 6.64 nCcm^{-2}. θ_C = 22.7°, δ_C =19.7°, $\Delta\varepsilon$ = -1.0. It was assumed B_3 = 5pN, B_{13} = 0pN. b) The effect of varying c-director bend and splay elastic constants B1 and B_2 on the tV characteristic. (d = 1.5μm, P_S = 5nCcm^{-2}, B_3=10pN, T_0=6×10^{-5}N/m, θ_C=25°, δ_C =21°, $\partial\varepsilon$=+0.5, $\Delta\varepsilon$= -1)

The combination of C2 alignment, high dielectric biaxiality and the mono-polar scheme act to greatly enhance discrimination between select and non-select resultants, as described in section 2. However, as is evident from figure 22a, commercially available liquid crystal materials such as SCE8 were inherently too slow and operated at voltages far above those provided by conventional display drivers. The development of new materials and mixtures was essential before the 15μs per line response time target could be achieved. To enable this, a simple set of material design rules was needed, including rules to maximise the dielectric biaxiality. Simplifying equations (38) and (48) gives the approximate relationship:

$$\partial\varepsilon \sim \frac{N}{T}\mu_\perp^2 C \sim \mu_\perp^2 \sin^2\theta_C \tag{52}$$

which can be used as a tool to help formulate improved materials. Assuming that the biaxial order parameter C is similar for all $S_C(*)$ materials for a given temperature below the Curie point T_C, achieving low voltage τV_{min} requires high transverse dipole moment $\mu_\perp$. The key to successful mixture design is then to ensure that this is done without concomitant increase of viscosity, as well as achieving the required phase sequence and transition temperatures, optical properties and stability. Remarkably, and typical of the Hull group, it was George Gray, with his team of Ken Toyne, Dave Lacey and Mike Hird who made the most significant $S_C(*)$ material breakthrough through the development of the 2,3 substituted di-fluoro terphenyls and biphenyls [45].
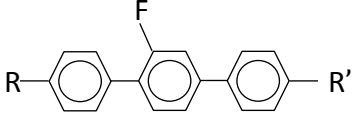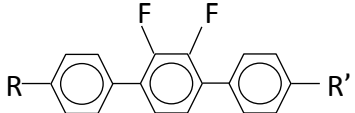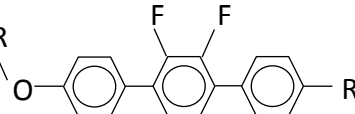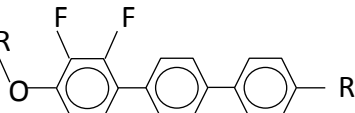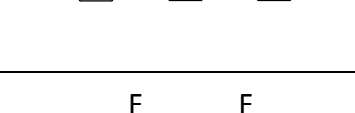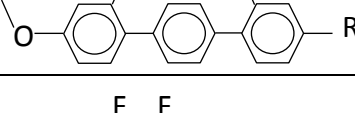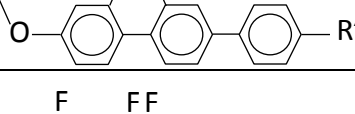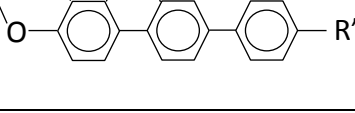
Dielectric biaxialities were measured for a variety of host materials from various groups [38], but it was Hull's di-fluoroterphenyls that gave the highest values. Having completed my initial work on determining the dielectric biaxialities for the various S_C hosts, I was ready to hand the first draft of my Doctorate dissertation to my Chemical supervisors, John Goodby and George Gray. However, Peter Raynes suggested that the work was rather light on chemistry: to placate George and John, I undertook a series of dielectric, dipole moment and viscosity measurements for a range of compounds synthesised at Hull. Table 1 shows some of the fluorinated terphenyl results. The measurements were determined from extrapolation of low concentrations

of each compound in the isotropic liquid PCH-32. The dipole moments were found by from dielectric and refractive index measurements in the manner of reference [46].

These measurements showed that the viscosity was lowest for the di-alkyl terphenyls fluorinated on the central ring, and that the inclusion of an alkoxy group, or positioning the 2,3 difluoro group on the end ring doubled the viscosity. The position of the 2,3 difluoro group did not influence the dipole moment at all for the di-alkyl terphenyl, but caused an increase from 10.8×10^{-30}Cm to 12.8×10^{-30}Cm when attached adjacent to a terminal alkoxy- chain (compare compounds 2 and 3 in table 1). Table 1 also includes estimates of what the dipole moments would be given free rotation (where the total dipole moment is given by the root-mean-square of the individual dipoles), or hindered rotation in either parallel or antiparallel orientations. Comparison of the mono- and di- fluoro terphenyls compound 1 and 2, allows the individual and transverse dipole moments of the fluorinated phenyl moiety to be found as 5.05×10^{-30}Cm to 12.8×10^{-30}Cm. The alkoxy group also has a strong perpendicular dipole moment, measured as 4.1×10^{-30}Cm. Measurements were made for a series of fluorinated terphenyls, including compounds 5, 6, and 7 of table 1. These suggested that the distribution of dipoles on different phenyl groups was randomly oriented with respect to each other through free rotation of the phenyl groups, unless attached in the 2,3' position of adjacent phenyls as in compound 7. The additive nature of dipoles on adjacent phenyl groups was subsequently utilised through the synthesis of tri-fluoro terphenyls [47] such as compound 8. Not only did these compounds have very high transverse dipole moments, they were also found to exhibit low viscosities and melting points [48]. Similar ideas were used to further increase the transverse dipole by including further fluorination in the terminal end chain, such as for compound 9 in table 1 [49] which achieved a significantly higher transverse dipole moment than could be achieved with cyano- substitution and with far lower viscosities.

Table 1   The dipole moments of several difluorinated terphenyl compounds.

	Compound structure	$\Delta\varepsilon$ $\pm$ 0.2	η / cP	Dipole moment μ / $\times 10^{-30}$ Cm			
				Measure ±0.4	Estimates	$\mu_{\perp}$	Theory DFT
1	(structure: R—⬡—⬡(F)—⬡—R′)	0.0	45	7.3	$\sqrt{5.3^2 + 5.05^2}=7.3$	5.05	0.6
2	(structure: R—⬡—⬡(F F)—⬡—R′)	-2.0	40	10.1	$5.05+5.05=10.1$	10.1	6.8
3	(structure: R-O—⬡—⬡(F F)—⬡—R′)	-2.0	70	10.8	$\sqrt{4.1^2 + 10.1^2}=10.9$	10.9	8.5
4	(structure: R-O—⬡(F F)—⬡—⬡—R′)	-4.2	200	12.8	$\sqrt{4.1^2 + 10.1^2}=10.9$ $10.1 + 4.1 = 14.2$	14.2	8.8
5	(structure: R-O—⬡(F)—⬡—⬡(F)—R′)	-1.1		11.5	$\sqrt{(4.1 + 5.05)^2 + 10.6^2 + 5.05^2} = 14.9$ $\sqrt{4.1^2 + 10.6^2} = 11.4$	10.4 4.1	11.2
6	(structure: R-O—⬡(F)—⬡—⬡(F)—R′)	-1.2		8.9	$\sqrt{4.1^2 + 5.05^2 + 5.05^2} = 8.3$	8.2	9.0
7	(structure: R-O—⬡(F F)—⬡—⬡—R′)	-1.8		9.5	$\sqrt{4.1^2 + 10.1^2} = 10.9$	10.9	
8	(structure: R-O—⬡(F F F)—⬡—⬡—R′)	-4.5	150	15.2	$\sqrt{(12.8 + 5.05)^2 + 5.3^2} = 18.6$ $\sqrt{12.8^2 + 5.05^2 + 5.3^2} = 14.7$	16.7 13.8	14.7
9	(structure: R—⬡(F F F F)—⬡—⬡—O—R′)	-5.5	250	24.5			

60

These results helped guide the design of superior mixtures for τV_{min} FLC applications Figure 24 shows the composition and results for the mixtures FDD12, [50]: latching with 5μs, 40V pulses is achieved in a 1.3μm device. This translates to sub-40V addressing times below the 12μs target for HDTV. The base host uses di-alkyl di-fluoroterphenyl (compound 2) to give low viscosity and wide smectic C phase whilst exhibiting a medium dielectric biaxiality. Such compounds are strongly S_C to N in nature, and so the smectic A phase is induced by adding in low viscosity phenyl pyrimidine because these compounds tend to exhibit an S_C to S_A phase sequence. The high biaxiality is then induced through the addition of S_C forming high transverse dipole moment compounds, such as 4, 8 or 9 [51], together with a small amount of a long pitch chiral dopant to induce the ferroelectric spontaneous polarisation.
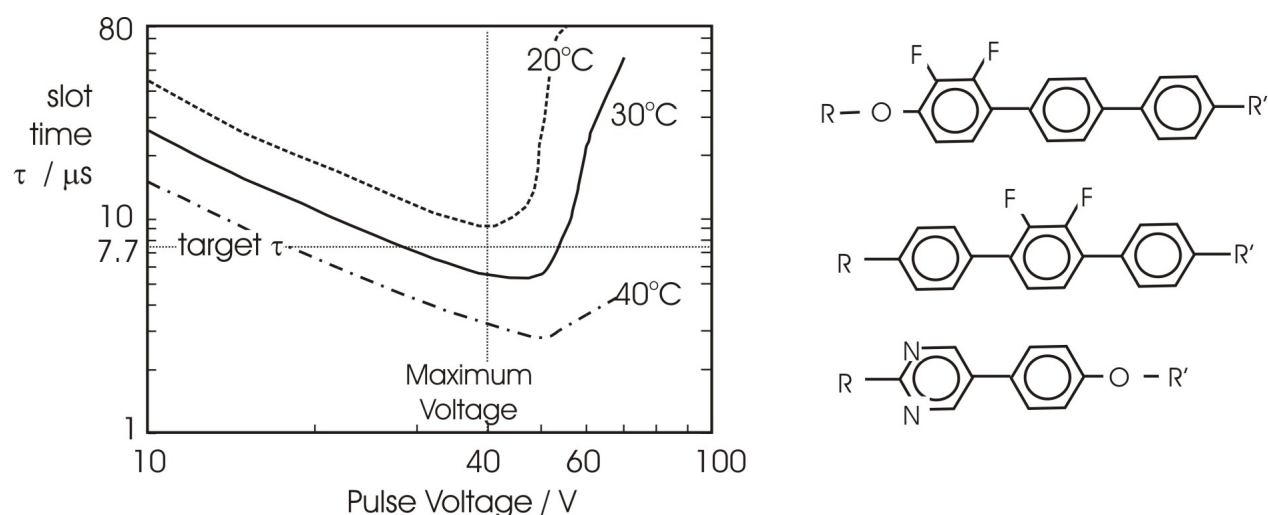
Figure 24. Low viscosity high dielectric biaxiality mixtures for use in τV_{min} SSFLC [50].

6   Conclusion

Figure 25 shows an example ¼ HDTV image displayed on the Sharp / DRA panel of reference [31]. Despite achieving a 150 : 1 contrast ratio , a 15% brightness efficiency yielding 200 Cdm^{-2}, and the 60Hz frame rate from 0°C to 60°C, the display cost and yield were not competitive with the burgeoning TFT solution beginning to emerge at the end of the 1990s. Although testament to the potential of bistable LCD, the advent of the low cost TFT driven display means there is no longer a need for a passive matrix video-rate display technology. FLC applications are restricted to those where image storage or fast frame rate active matrix is required: for such applications C1 or quasi-bookshelf geometries are preferable to C2.

But the story does not end there. It is interesting to note that many modern LCD HDTV are based on vertically aligned nematic modes that require a high negative dielectric anisotropy combined with low viscosity. The compounds that George Gray helped create, either directly or through his research students, are used in these modes [52]. His influence on the world of LCD, therefore, is as strong today, as it was for his cyano-biphenyls that initiated the industry in the 1970s.

Figure 25. ¼ HDTV image displayed on the 17" DRA / Sharp tV$_{min}$ Panel.

Acknowledgements

References

[1] Surguy PWH, Ayliffe PJ, Birch MJ, Bone MF, Coulson I, Crossland W A., Hughes JR, Ross PW, Saunders FC, Towler MJ. The "JOERS/Alvey" ferroelectric multiplexing scheme. Ferroelectrics. 1991;122:63–79.

[2] Jones JC, Towler MJ, Hughes JR. Fast, high-contrast ferroelectric liquid crystal displays and the role of dielectric biaxiality. Displays. 1993;14:86–93.

[3] Clark N and., Lagerwall ST. Submicrosecond bistable electro-optic switching in liquid crystals. Appl Phys Lett. 1980; 36:899–901.

[4] Blinov LM, Palto SP. A New Insight on the Bistability and Relevant Phenomena in Ferroelectric Smectic C* Liquid Crystals. Mol Cryst Liq Cryst. 2005; 429: 31–53.

[5] Available from E. Merck

[6] Rieker TP, Clark NA, Smith GS, Parmar DS, Sirota EB, Safinya CR. "Chevron" Local Layer Structure in Surface-Stabilized Ferroelectric Smectic-C Cells. Phys Rev Lett. 1987; 59: 2658.

[7] Kanbe J, Inoue H, Mizutome A, Hanyuu Y, Katagiri K, Yoshihara S. High resolution, large area FLC display with high graphic performance. Ferroelectrics. 1991; 114: 3–26.

[8] Jones JC. The relationship between the smectic C director and layer profiles and the surface anchoring energies. Ferroelectrics. 1996; 178:155–65.

[9] Brown CV, Dunn PE, Jones JC, Jenkins SA, Richardson RM. X-Ray Structural Studies of Ferroelectric Liquid Crystal Devices. Mol Cryst Liq Cryst. 2003; 402:55–75.

[10] Brown CV, Dunn PE, Jones JC. The effect of the elastic constants on the alignment and electro-optic behaviour of smectic C liquid crystals. Euro J Appl Math 1997;8 281–91.

[11] Yang KH, Lien A, Chieu TC. Optical methods for the measurement of layer-tilt and pretilt angles in surface-stabilized ferroelectric liquid crystal devices. Japanese J Appl Physics, Part 1. 1988; 27:2022–5.

[12] Clark NA. Rieker TP, Maclennan JE Director and layer structure of SSFLC cells. Ferroelectrics. 1988; 85:79–97.

[13] Orsay group on Liquid Crystals Simplified elastic theory for smectic C," Solid State. Commun. *1971:* 9, 653-655.

[14] Leslie, FM Stewart, IW and Nakagawa M A continuum theory for smectic C liquid crystals, Mol. Cryst. Liq. Cryst. 1991: 198, 443 – 454.

[15] Leslie FM, Stewart IW, and Nakagawa M Equivalent smectic C Liquid Crystal Energies, Cont. Mech. Thermodyn. 1991*:* 3, 237 – 250.

[16] McKay G and Leslie FM "A continuum theory for smectic liquid crystals allowing layer dilation and compression," Euro. J. Appl. Math*,* 1997: 8, 3, 273 – 280.

[17] Anderson MH, Jones JC, Raynes EP and Towler MJ Optical studies of thin layers of smectic-C materials, J. Appl. Phys., 1991**:** 24, 338-342.

[18] Taylor TR, Fergason JL and Arora, SL (1970). Biaxial liquid crystals. Phys. Rev. Lett, 1970: *24* (8), 359–362.

[19] Lockhart TE, Allender DW, Gelerinter E and Johnson, DL Investigation of the indices of refraction near the smectic-A to smectic-C transition: Orientational order. Phys. Rev. A, 1979: *20* (4), 1655–1660.

[20] Jones JC, Raynes, EP, Towler, MJ and Sambles JR Observation of Dielectric Biaxiality in a Two-Frequency Smectic-C and a Reinterpretation of Ferroelectric Liquid Crystal AC Field Effects Mol. Cryst. Liq. Cryst. Lett. 1990: 7 (3) 91-99.

[21] Jones JC and Raynes EP, Measurement of the Biaxial Permittivities for Several Smectic-C Host Materials used in Ferroelectric Liquid Crystals Devices, Liquid Crystals 1991**.** 11, (10), 199 - 217.

[22] Geary JM, SID Digest of Papers 1985: 128- 131

[23] Takatoh K, Hasegawa M, Koden M, Itoh N, Hasegawa R and Sakamoto M, Alignment Technologies and Applications of Liquid Crystal Devices", 1985: *Taylor and Francis*, London.

[24] Jones JC, Towler MJ, and Raynes EP, "The importance of dielectric biaxiality for ferroelectric liquid crystal devices", Ferroelectrics, 1991: 121 (2) 91 – 102.

[25] Vaupotič N, Kralj S, Copič M, Sluckin TJ Phys. Rev E., 1996: 54, *3783*

[26] Webster RE, Mottram NJ, Cleaver DJ. Molecular simulation of chevrons in confined smectic liquid crystals. Phys Rev E Stat Nonlin Soft Matter Phys. 2003; 68:021706.

[27] Mottram, NJ, Ul Islam N and Elston SJ, Biaxial modeling of the structure 1of the Chevron Interface in Smectic Liquid Crystals, Phys. Rev. E, 1999: 60: 613 - 619.

[28] Saunders FC, Hughes JR, Pedlingham HA, and Towler MJ "Electro-optic response of Ferroelectric Liquid Crystals", Liq. Cryst., 1989: **6**,(3) 341 – 347.

[29] Jones JC, Brown CV and Dunn PE The Physics of τVmin Ferroelectric Liquid Crystals Ferroelectrics, 2000: 246, 191 – 201.

[30] Bradshaw MJ, Brown CV, Haslam SD, Hughes JR, Graham A, Jones JC, Katsuse H, Kawabata Y, Koden M, Miyoshi S, Nonomura K, Numao T, Shigeta M, Sugino M, Tagawa A, Gass PA, Raynes EP, Towler MJ. Key Technologies for τVmin FLCDs. Proc. Intl. Disp. Res. Conf. Toronto, Canada. 1997. L16–L17.

[31] Itoh N, H.Akiyama, Kawabata Y, Koden M, Miyoshi S, Numao T, Shigeta M, Bradshaw MJ, Brown CV, Graham A, Haslam SD, Hughes JR, Jones JC, Slaney AJ, Bonnett P, Gass PA, Raynes EP, Ulrich DC. 17" Video-rate Full Colour FLCD. Proc. Int. Displays Work. (IDW), Kobe, Japan, December 1998. 1998; PLC 1–2. 205–pp208.

[32] Koden M, Miyoshi S. Ferroelectric Liquid Crystal Display. Sharp Tech. J. 1997;1:2–7.

[33] Koden M. Passive-matrix FLCDs with high contrast and video-rate full-color pictures. Ferroelectrics. 2000;246:87–96.

[34] Jones C. Bistable Nematic Liquid Crystal Displays. In: Goodby JW, Collings PJ, Kato T, Tschierske C, Gleeson H, Raynes P, editors. Handb. Liq. Crystals, Vol. 8. Wiley VCH; 2013.

[35] Hughes JR, Raynes EP. A new set of high speed matrix addressing schemes for ferroelectric liquid crystal displays. Liq. Cryst. 1993;15:281–282.

[36] M.H. Anderson, Hughes JR, Jones JC, Russell KG. Comparison of Three Slot DRAMA with other τVmin Drive schemes. Proc. 14th Intl. Disp. Res. Conf. (IDRC '97). 1997. p. L40–L41.

[37] Yang F and Sambles, JR Critical Angles for Reflectivity at an Isotropic-anisotropic Boundary. J. Mod. Optics, 1993: *40* (6), 1131–1142.

[38] Jones, J.C. Optical and Dielectric Studies of Smectic C Liquid Crystals. *Ph .D Thesis*, 1991: University of Hull, UK.

[39] Dunn PE. Physical Properties of Smectic C Liquid Crystals. *Ph. D Thesis*, 1998: University of Bristol, UK.

[40] Gouda F, Kuczynski W, Lagerwall ST, Matuszczyk M, Matuszczyk T and Skarp K, Determination of the dielectric biaxiality in a chiral smectic-C phase. Phys. Rev. A, 1992: 46(2), 951

[41] Brown CV and Jones JC Accurate determination of the temperature and frequency dependent smectic C biaxial permittivity tensor. J. Appl. Phys. 1999; 86: 3333 - 3341.

[42] Straley JP Ordered phases of a liquid of biaxial particles Phys. Rev. A. 1974: 1881 − 1887

[43] Toriyama K, Dunmur DA and Hunt SE, Transverse dipole association and negative dielectric anisotropy of nematic liquid crystals. Liquid Crystals, 2015: 1001–1009.

[44] Raynes EP The Chemistry and Physics of Thermotropic Liquid Crystals IN Gunter P "Electro-optic and Photo refractive materials" 1986 *Springer Verlag.* 80 – 89

[45] Gray GW, Hird M, Lacey D, Toyne KJ. The Synthesis and Transition Temperatures of some 4,4" Dialkyl and 4,4" Alkoxyalkyl-1,1':4',1" - terphenyls with 2,3 or 2'3' diFluoro Substituents and of their Biphenyl Analogues. J Chem Soc Perkin Trans II. 1989; 2041–53.

[46] Raynes EP. The Measurement of Molecular Dipole Moments of Liquid Crystals. Mol. Cryst. Liq. Cryst. Lett. 1985;1:69–74.

[47] Jones JC, Slaney AJ, Hird M, Glendenning ME, Goodby JW, Toyne KJ, Lewis RA, Gough N. Fluorinated Terphenyls. 1998 *Patent GB 9815536.9*

[48] Hird M. Ferroelectricity in liquid crystals—materials, properties and applications. *Liq Cryst* 2011 : 38 (11-12) 37–41.

[49] Jones JC, Sage IC, Goodby JW, Hird M, Lewis RA, Toyne KJ. High transverse dipole moment aryl compounds. 2002. *Patent GB 9815536.9*

[50] Slaney AJ, Minter V, Jones JC. Assessing ferroelectric materials for application in τV_{MIN} Mode Devices. *Ferroelectrics*. 1996; 178: 65–74.

[51] Jones JC, Slaney AJ. Liquid Crystal composition and liquid crystal shutter. 2001. *US Patent 6280653*

[52] Gasowska JS, Cowling SJ, Cockett MCR, Hird M, Lewis R A., Raynes EP, Goodby JW. The influence of an alkenyl terminal group on the mesomorphic behaviour and electro-optic properties of fluorinated terphenyl liquid crystals. J. Mater. Chem. 2010: 20:299.